

---

# Value Gradient Sampler: Sampling as Sequential Decision Making

---

Sangwoong Yoon<sup>\*1</sup> Himchan Hwang<sup>\*2</sup> Hyeokju Jeong<sup>\*2</sup> Dong Kyu Shin<sup>\*2</sup> Che-Sang Park<sup>2</sup> Sehee Kweon<sup>3</sup>  
Frank Chongwoo Park<sup>2,3</sup>

## Abstract

We propose the Value Gradient Sampler (VGS), a trainable sampler based on the interpretation of sampling as discrete-time sequential decision-making. VGS generates samples from a given unnormalized density (i.e., energy) by drifting and diffusing randomly initialized particles. In VGS, finding the optimal drift is equivalent to solving an optimal control problem where the cost is the upper bound of the KL divergence between the target density and the samples. We employ value-based dynamic programming to solve this optimal control problem, which gives the gradient of the value function as the optimal drift vector. The connection to sequential decision making allows VGS to leverage extensively studied techniques in reinforcement learning, making VGS a fast, adaptive, and accurate sampler that achieves competitive results in various sampling benchmarks. Furthermore, VGS can replace MCMC in contrastive divergence training of energy-based models. We demonstrate the effectiveness of VGS in training accurate energy-based models in industrial anomaly detection applications.

## 1. Introduction

Generating samples from an unnormalized target density function is a fundamental task in probabilistic inference, and its applications are encountered across diverse fields, including machine learning (Hinton, 2002), statistical mechanics (Noé et al., 2019), particle physics (Heimel et al., 2023) and computational chemistry (Leimkuhler & Matthews, 2015). While Markov Chain Monte Carlo (MCMC) has been the standard approach for sampling, it often requires a very long chain to generate independent samples for high-dimensional

---

<sup>\*</sup>Equal contribution <sup>1</sup>University College London, London, UK <sup>2</sup>Seoul National University, Seoul, Republic of Korea <sup>3</sup>Saige Co., Ltd, Seoul, Republic of Korea. Correspondence to: Sangwoong Yoon <sangwoong.yoon@ucl.ac.uk>, Frank C. Park <fcp@snu.ac.kr>.

Preprint

multi-model densities. A neural network trained as a sampler serves as an efficient alternative to MCMC, enabling the fixed-time generation of new samples.

Viewing sampling as an optimal control problem is an emerging approach for training neural samplers (Zhang & Chen, 2022; Berner et al., 2022; Vargas et al., 2023). In many conventional sampling methods, such as MCMC, a sample is generated through multiple displacement steps from a point drawn from a prior distribution. Therefore, it is natural to ask whether we can find a policy that optimally moves the particle. Formulating a sampling problem as optimal control provides a systematic framework to build a novel class of samplers and opens up interesting connections to other important ideas in machine learning, such as diffusion modeling (Berner et al., 2022; Phillips et al., 2024; Huang et al., 2024; McDonald & Barron, 2022) and Schrödinger bridge (Vargas et al., 2023).

The existing optimal control samplers are typically formulated using stochastic differential equations (SDEs) and, therefore, defined in *continuous-time*. While SDE-based formulations are elegant and provide strong mathematical claims, they face several challenges when deployed in practice. First, generating a new sample requires many simulation steps and is thus slow. An accurate simulation of continuous-time dynamics requires fine-grained discretization with more than a hundred steps. Second, optimal control samplers rely on Neural SDEs (Kidger et al., 2021a; Tzen & Raginsky, 2019), whose stable and efficient optimization is non-trivial (Kidger et al., 2021b).

In this paper, we demonstrate that directly solving optimal control in a *discrete-time* setting can be more effective and practical. A discrete-time policy can be directly optimized for fewer time steps, minimizing the performance degradation from discretization. Furthermore, discrete-time optimal control can be written as a Markov Decision Process (MDP). This allows us to use well-established techniques in sequential decision making and reinforcement learning (RL) for effective and efficient optimization.

We propose the **Value Gradient Sampler** (VGS) as an instantiation of a sequential decision-making approach for sampling. Like Langevin Monte Carlo and diffusion models, VGS applies drift and diffusion processes  $T$  times to

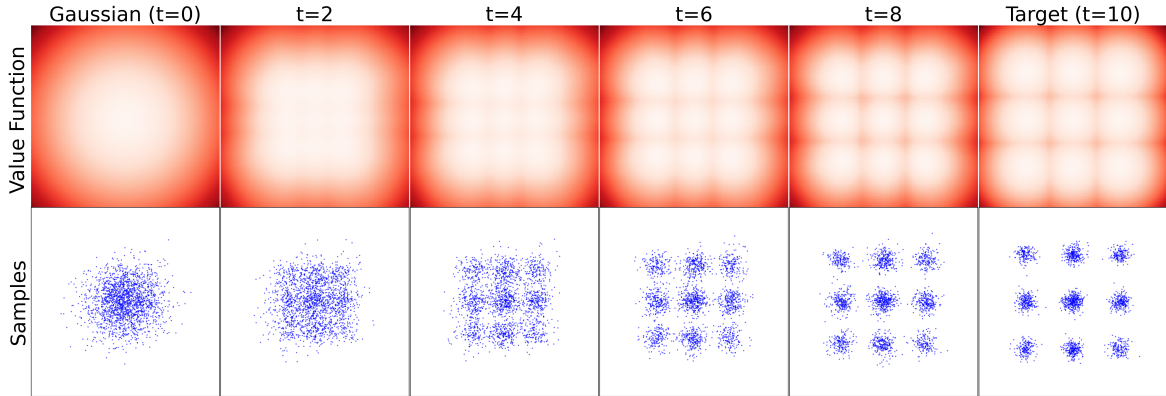


Figure 1. VGS trained on a mixture of 9 Gaussians with  $T = 10$ . The value functions and corresponding samples at each time step are shown. Samples drift along the gradient of the next-step value function. The experimental setup and results are explained in Section 7.1.

a randomly initialized particle to generate a sample. The drift vector is determined by minimizing the upper bound of the KL divergence between the samples and the target density, which takes the form of a classical optimal control objective.

We employ value-based dynamic programming to solve this optimal control problem, yielding the gradient of the value function as the optimal drift vector. The value function is represented by a neural network and trained using standard RL techniques, such as temporal difference learning. We evaluate VGS on multiple sampling benchmarks, including sampling equilibrium states of a  $n$ -body system. VGS demonstrates competitive performance, often outperforming SDE-based samplers which use significantly larger  $T$ .

In addition to sampling, VGS can be utilized to train energy-based models (EBMs). The maximum likelihood training of an EBM is known to be highly unstable and computationally intensive due to the need for MCMC as a subroutine (Hinton, 2002; Du & Mordatch, 2019; Yoon et al., 2021). We demonstrate that VGS can replace MCMC in EBM training, making the process more efficient and resulting energy more accurate energy estimates.

The contribution of the paper can be summarized as follows:

- We propose the Value Gradient Sampler (VGS), a sampler trained via RL.
- We demonstrate that VGS can generate new samples faster than SDE-based samplers while maintaining the quality of samples.
- We show that replacing MCMC with VGS produces a more accurate energy function, improving the performance of energy-based anomaly detection.

Code is available at <https://github.com/swyoon/value-gradient-sampler/>.

## 2. Preliminaries

**Sampling Problems.** We consider the problem of drawing independent samples from a target density function  $q(\mathbf{x})$  defined in  $\mathbb{R}^D$ . Assuming  $q(\mathbf{x}) > 0$  for all  $\mathbf{x}$ , the target density can be expressed as:

$$q(\mathbf{x}) = \frac{1}{Z} \exp(-E(\mathbf{x})/\tau), \quad (1)$$

where  $E : \mathbb{R}^D \rightarrow \mathbb{R}$  is called an energy function,  $\tau > 0$  is a temperature parameter, and  $Z$  is the normalization constant. The function  $E(\mathbf{x})$  is assumed to be differentiable. The focus is on settings where the normalization constant  $Z$  is unknown or difficult to compute, with access limited to  $E(\mathbf{x})$  and  $\tau$ .

One of the most widely adopted sampling methods is MCMC, which utilizes a Markov chain having  $q(\mathbf{x})$  as the stationary distribution. However, obtaining a sample in MCMC is slow because a large number of iterations have to be conducted for every independent sample generation.

**Training Parametric Samplers.** We aim to train a parametric sampler  $\pi_\phi(\mathbf{x})$  with parameter  $\phi$  to generate approximate samples from the target density  $q(\mathbf{x})$ . A parametric sampler can be faster at generating new samples as computation can be amortized in the training phase.

A natural choice of the objective function is the KL divergence between  $\pi_\phi(\mathbf{x})$  and  $q(\mathbf{x})$ :

$$\min_{\phi} KL(\pi_\phi(\mathbf{x})||q(\mathbf{x})) = \min_{\phi} \mathbb{E}_{\pi_\phi} \left[ \log \frac{\pi_\phi(\mathbf{x})}{q(\mathbf{x})} \right], \quad (2)$$

which does not require samples from  $q(\mathbf{x})$  for training.

**Sampler Model.** In this work, the sampler distribution  $\pi_\phi(\mathbf{x})$  is implicitly obtained by the result of the following iterative drift-diffusion process:

$$\mathbf{x}_0 \sim \mathcal{N}(0, \sigma_{init}^2 I), \quad \mathbf{x}_{t+1} = \alpha_t \mathbf{x}_t + \mu_\phi^t(\mathbf{x}_t) + \sigma_t \epsilon_t \quad (3)$$

**Algorithm 1** Value Gradient Sampling

---

**Input:** Value  $V_\phi^t(\mathbf{x}_t)$ ,  $\{\alpha_t\}_{t=0}^{T-1}$ ,  $\{s_t\}_{t=0}^{T-1}$ ,  $\sigma_{init}$   
 $x_0 \sim \mathcal{N}(0, \sigma_{init}^2 I)$  // Initialize samples  
**for**  $t = 0$  **to**  $T - 1$  **do**  
 $\mu_\phi^t(\mathbf{x}_t) = -\frac{s_t^2 \alpha_t^2}{\tau} \nabla V_\phi^{t+1}(\alpha_t \mathbf{x}_t)$ ,  $\sigma_t = \alpha_t s_t$  // Eq. (12)  
 $\mathbf{x}_{t+1} = \alpha_t \mathbf{x}_t + \mu_\phi^t(\mathbf{x}_t) + \sigma_t \epsilon_t$  // Eq. (3)  
**end for**  
**Output:**  $\{\mathbf{x}_t\}_{t=0}^T$

---

for  $t = 0, \dots, T - 1$ . The coefficients  $\alpha_t$  and  $\sigma_t$  are constants and  $\epsilon_t \sim \mathcal{N}(0, I)$ . The drift  $\mu_\phi^t(\mathbf{x}_t)$  is a function of  $\mathbf{x}_t$  and  $t$ , parametrized by  $\phi$ . We set  $\pi_\phi(\mathbf{x})$  to refer to the distribution of the final particle  $\mathbf{x}_T$ . We will often write the final particle  $\mathbf{x}_T$  as  $\mathbf{x}$ , dropping the subscript.

The drift-diffusion process in Equation (3) is a Markov process. The transition dynamics becomes that of Langevin Monte Carlo (Roberts et al., 1996) when  $\alpha_t = 1$  and  $\mu_\phi^t(\mathbf{x}_t) = (\sigma_t^2/2) \nabla_{\mathbf{x}_t} \log q(\mathbf{x}_t)$ . A diffusion model (Ho et al., 2020; Song et al., 2021) can also be expressed in the same form, where the drift is the score of the diffused version of  $q(\mathbf{x})$ . Finally, Equation (3) can be viewed as the discretization of SDE via the Euler-Maruyama method.

However, since  $\pi_\phi(\mathbf{x})$  is defined implicitly, training the distribution by  $\min_\phi KL(\pi_\phi(\mathbf{x}_T) || q(\mathbf{x}_T))$  is not trivial due to two challenges. First, the entropy of the sample distribution  $\pi_\phi(\mathbf{x})$  is not analytically computable. Second, the gradient must propagate through time, requiring significant memory and making it vulnerable to gradient explosion or vanishing.

### 3. Value Gradient Sampling

Here, we propose the **Value Gradient Sampler** (VGS), a novel sampler that interprets the drift-diffusion process (Equation (3)) as a sequential decision-making problem.

#### 3.1. Sampling as Optimal Control

Instead of solving  $\min_\phi KL(\pi_\phi(\mathbf{x}_T) || q(\mathbf{x}_T))$  directly, we minimize its upper bound. The upper bound is obtained by the data processing inequality, allowing the incorporation of intermediate diffusion steps  $\mathbf{x}_{0:T-1}$  into the KL divergence:

$$KL(\pi_\phi(\mathbf{x}_T) || q(\mathbf{x}_T)) \leq KL(\pi_\phi(\mathbf{x}_{0:T}) || \tilde{q}(\mathbf{x}_{0:T})), \quad (4)$$

where we also introduce an auxiliary distribution  $\tilde{q}(\mathbf{x}_{0:T}) = q(\mathbf{x}_T) \prod_{t=0}^{T-1} \tilde{q}(\mathbf{x}_t | \mathbf{x}_{t+1})$ . Note that the data processing inequality holds for an arbitrary choice of  $\tilde{q}(\mathbf{x}_t | \mathbf{x}_{t+1})$ .

Now the right-hand side of Equation (4) can be minimized:  $\min_\phi KL(\pi_\phi(\mathbf{x}_{0:T}) || q(\mathbf{x}_T) \tilde{q}(\mathbf{x}_{0:T-1} | \mathbf{x}_T))$ . By plugging the definitions of each distribution, multiplying by  $\tau$ , and

**Algorithm 2** Learning Value Functions in VGS

---

**Input:** Energy  $E(\mathbf{x})$ , value  $V_\phi^t(\mathbf{x}_t)$ , target value  $V_{\phi^-}^t(\mathbf{x}_t)$ , hyperparameters  $\alpha_t, s_t, \sigma_{init}, n_{update}$   
**repeat**  
 Sample  $\{(\mathbf{x}_t, \mu_{\phi^-}^t(\mathbf{x}_t))\}_{t=0}^T$  using  $V_{\phi^-}$  // Alg. 1  
 Initialize replay buffer  $\mathcal{D} = \{(\mathbf{x}_t, \mu_{\phi^-}^t(\mathbf{x}_t))\}_{t=0}^T$   
**for**  $i = 1$  **to**  $n_{update}$  **do**  
   **for**  $(\mathbf{x}_t, \mu_{\phi^-}^t(\mathbf{x}_t))$  **in**  $\mathcal{D}$  **do**  
      $\mathbf{x}_{t+1} = \alpha_t \mathbf{x}_t + \mu_{\phi^-}^t(\mathbf{x}_t) + \sigma_t \epsilon_t$  // Eq. (3)  
     Compute  $TD(\mathbf{x}_t, \mathbf{x}_{t+1})$  // Eq. (13)  
     Optimize  $\min_\phi ((V_\phi^t(\mathbf{x}_t) - TD(\mathbf{x}_t, \mathbf{x}_{t+1}))^2)$   
   **end for**  
**end for**  
 $\phi^- \leftarrow \lambda \phi^- + (1 - \lambda) \phi$   
 update  $\sigma_{init}$  // Eq. (39)  
**until** Convergence

---

discarding all constants, following problem is obtained:

$$\min_\phi \mathbb{E}_{\pi_\phi(\mathbf{x}_{0:T})} \left[ E(\mathbf{x}_T) + \tau \sum_{t=0}^{T-1} \log \frac{\pi_\phi(\mathbf{x}_{t+1} | \mathbf{x}_t)}{\tilde{q}(\mathbf{x}_t | \mathbf{x}_{t+1})} \right], \quad (5)$$

which can be viewed as an optimal control problem. The controller  $\pi_\phi(\cdot)$  is optimized to minimize the terminal cost  $E(\mathbf{x}_T)$  plus the running costs  $\log \pi_\phi(\mathbf{x}_{t+1} | \mathbf{x}_t) / \tilde{q}(\mathbf{x}_t | \mathbf{x}_{t+1})$  for each transition  $(\mathbf{x}_t, \mathbf{x}_{t+1})$ . The temperature  $\tau$  balances between the terminal and the running costs. To solve this standard optimal control problem, we apply the classical value-based dynamic programming approach.

**Value Function.** A value function, or cost-to-go function,  $V_\pi^t(\mathbf{x}_t)$  is defined as the expected sum of the future costs starting from  $\mathbf{x}_t$ , following  $\pi$ .

$$V_\pi^t(\mathbf{x}_t) = \mathbb{E}_\pi \left[ E(\mathbf{x}_T) + \tau \sum_{t'=t}^{T-1} \log \frac{\pi_\phi(\mathbf{x}_{t'+1} | \mathbf{x}_{t'})}{\tilde{q}(\mathbf{x}_{t'} | \mathbf{x}_{t'+1})} \middle| \mathbf{x}_t \right] \quad (6)$$

for  $t = 0, \dots, T - 1$ . We set  $V_\pi^T(\mathbf{x}_T) = E(\mathbf{x}_T)$ . The optimal value function  $V_*^t(\mathbf{x}_t)$  is a value function that satisfies the Bellman optimality equation (Appendix A). In practice, a value function is approximated with a neural network that takes  $(\mathbf{x}_t, t)$  as input and returns a scalar.

#### 3.2. Value Gradient Sampler

We present VGS, a sampler that (approximately) solves the optimal control objective (Equation (5)) by drifting a particle along the gradient of the next-step value function. First, it is assumed that our policy  $\pi(\mathbf{x}_{t+1} | \mathbf{x}_t)$  follows the drift-diffusion process in Equation (3) such that

$$\pi(\mathbf{x}_{t+1} | \mathbf{x}_t) = \mathcal{N}(\mathbf{x}_{t+1}; \alpha_t \mathbf{x}_t + \mu_t, \sigma_t^2 I). \quad (7)$$

We will find the drift vector  $\mu_t$  and the noise magnitude  $\sigma_t$  that solves Equation (5) as optimally as possible.

For now, we assume that the value function at time  $t + 1$ ,  $V_\pi^{t+1}(\mathbf{x}_{t+1})$ , is given, and the policy  $\pi$  after  $t + 1$  is fixed. Note that the value function becomes the optimal value function when  $\pi$  is the optimal policy. Then, employing the dynamic programming approach, we focus on the subproblem of finding the optimal policy at time  $t$ .

$$\begin{aligned} \min_{\pi(\mathbf{x}_{t+1}|\mathbf{x})} \mathbb{E}_\pi \left[ E(\mathbf{x}_T) + \tau \sum_{t'=t}^{T-1} \log \frac{\pi(\mathbf{x}_{t'+1}|\mathbf{x}_{t'})}{\tilde{q}(\mathbf{x}_{t'}|\mathbf{x}_{t'+1})} \middle| \mathbf{x}_t \right] \quad (8) \\ = \min_{\pi(\mathbf{x}_{t+1}|\mathbf{x})} \mathbb{E}_\pi \left[ V_\pi^{t+1}(\mathbf{x}_{t+1}) + \tau \log \frac{\pi(\mathbf{x}_{t+1}|\mathbf{x}_t)}{\tilde{q}(\mathbf{x}_t|\mathbf{x}_{t+1})} \middle| \mathbf{x}_t \right] \end{aligned}$$

To fully specify the problem, the auxiliary distribution  $\tilde{q}(\mathbf{x}_t|\mathbf{x}_{t+1})$  has to be given. We choose  $\tilde{q}(\mathbf{x}_t|\mathbf{x}_{t+1})$  as the following distribution:

$$\tilde{q}(\mathbf{x}_t|\mathbf{x}_{t+1}) = \mathcal{N} \left( \frac{1}{\alpha_t} \mathbf{x}_{t+1}, s_t^2 I \right), \quad s_t > 0, \quad (9)$$

which later gives us a particularly simple solution and also has an interesting connection to both variance-exploding ( $\alpha_t = 1$ ) and variance-preserving ( $\alpha_t = 1/\sqrt{1-s_t^2}$ ) diffusion processes. Now we can write the optimization for  $\mu_t$  and  $\sigma_t$  as follows:

$$\begin{aligned} \min_{\mu_t, \sigma_t} \mathbb{E}_\epsilon \left[ V_\pi^{t+1}(\alpha_t \mathbf{x}_t + \mu_t + \sigma_t \epsilon) \right] \\ - \tau D \log \frac{\sigma_t}{s_t} + \frac{\tau \|\mu_t\|^2}{2s_t^2 \alpha_t^2} + \frac{\tau D \sigma_t^2}{2s_t^2 \alpha_t^2} - \tau \frac{D}{2}, \quad (10) \end{aligned}$$

where  $\epsilon \sim \mathcal{N}(0, I)$ . To handle the first term, we evaluate a first-order Taylor approximation of  $V_\pi^{t+1}$  around  $\alpha_t \mathbf{x}_t$ .

$$\begin{aligned} \mathbb{E}_\epsilon [V_\pi^{t+1}(\alpha_t \mathbf{x}_t + \mu_t + \sigma_t \epsilon)] \\ \approx V_\pi^{t+1}(\alpha_t \mathbf{x}_t) + \mu_t^\top \nabla_{\alpha_t \mathbf{x}_t} V_\pi^{t+1}(\alpha_t \mathbf{x}_t). \quad (11) \end{aligned}$$

Substituting the approximation into Equation (10) and setting the derivatives with respect to  $\mu_t$  and  $\sigma_t$  to zero, we obtain the analytic expressions for the optimal drift  $\mu_t$  and the optimal noise magnitude  $\sigma_t$  as follows:

$$\mu_t = -\frac{s_t^2 \alpha_t^2}{\tau} \nabla_{\alpha_t \mathbf{x}_t} V_\pi^{t+1}(\alpha_t \mathbf{x}_t), \quad \sigma_t = \alpha_t s_t. \quad (12)$$

The detailed derivation, including a second-order Taylor expansion, is presented in Appendix C. Note that  $\mu_t$  is now a function of  $\mathbf{x}_t$  and is fully determined by the value function. In practice, we will use the parametrized value function  $V_\phi^t(\mathbf{x}_t)$  with parameter  $\phi$  to approximate the value function and Equation (12) can also be used to sample using  $V_\phi^t(\mathbf{x}_t)$  as stated in Algorithm 1.

### 3.3. Training Value Functions Using RL

Since the optimal value function is not known in practice, we learn a value function through multiple evaluations of target energy  $E(\mathbf{x})$ . As described in Algorithm 2, we follow the framework of generalized policy iteration, which iterates between policy evaluation and policy improvement. Since the sampling step in VGS is equivalent to policy improvement, we discuss methods for policy evaluation.

**Temporal Difference Learning.** We implement temporal difference (TD) learning to evaluate the value function given samples from a policy. The value function needs to satisfy the following recurrence relation:

$$V_\pi^t(\mathbf{x}_t) = \mathbb{E}_{\pi(\mathbf{x}_{t+1}|\mathbf{x}_t)} \left[ V_\pi^{t+1}(\mathbf{x}_{t+1}) + \tau \log \frac{\pi(\mathbf{x}_{t+1}|\mathbf{x}_t)}{\tilde{q}(\mathbf{x}_t|\mathbf{x}_{t+1})} \middle| \mathbf{x}_t \right].$$

A parametric value function  $V_\phi^t(\mathbf{x}_t)$  is trained to minimize the discrepancy between the two sides of the recurrence relation. The TD target for  $V_\phi^t(\mathbf{x}_t)$  is expressed as:

$$TD(\mathbf{x}_t, \mathbf{x}_{t+1}) = V_\phi^{t+1}(\mathbf{x}_{t+1}) + \tau \log \frac{\pi_\phi(\mathbf{x}_{t+1}|\mathbf{x}_t)}{\tilde{q}(\mathbf{x}_t|\mathbf{x}_{t+1})}. \quad (13)$$

Then, the value function is trained by minimizing the TD error, the mean squared error to the TD target is:

$$\min_\phi \mathbb{E}_{\pi(\mathbf{x}_{t+1}|\mathbf{x}_t)} [(V_\phi^t(\mathbf{x}_t) - TD(\mathbf{x}_t, \mathbf{x}_{t+1}))^2], \quad (14)$$

where  $TD(\mathbf{x}_t, \mathbf{x}_{t+1})$  is treated to be independent of  $\phi$ . Note that other value function learning methods, e.g., Monte Carlo prediction, are also applicable to VGS.

**Target Network.** While Equation (14) works, often stability and performance can be improved by introducing a target network  $V_{\phi^-}^t(\mathbf{x}_t)$  to evaluate the TD target (Mnih et al., 2015). The target network parameter  $\phi^-$  is obtained via exponential moving averaging (EMA) of  $\phi$  from past iterations:  $\phi^- = \lambda \phi^- + (1 - \lambda) \phi$ . When a target network is employed for VGS, samples are generated using  $V_{\phi^-}^t(\mathbf{x}_t)$ .

**Replay Buffer.** For better sample efficiency, we utilize a replay buffer  $\mathcal{D}$  to store  $(\mathbf{x}_t, \mu_{\phi^-}^t(\mathbf{x}_t))$ , which allows us to resample  $\mathbf{x}_{t+1}$  during each update (Lin, 1992). Each sample is reused  $n_{update}$  times during training.

**Off-Policy Learning.** As in RL, off-policy data can be utilized in the value function learning. A particularly efficient and useful off-policy data is a trajectory collected from an amplified noise level  $(\sigma_t)_{\text{off}} = \eta \alpha_t s_t$  for a noise scale  $\eta > 1$ . Amplifying the noise roughly corresponds to sampling from a higher temperature and helps exploration.

### 3.4. Theoretical Analyses

In this section, we present two theoretical results regarding the optimal value function (Equation (6)) and the optimal

auxiliary distribution  $\tilde{q}(\mathbf{x}_{0:T})$ .

The first theorem demonstrates that the optimal value function can be interpreted as the energy of marginal density  $\tilde{q}(\mathbf{x}_t)$ , a diffused version of the target  $q(\mathbf{x}_T)$ .

**Theorem 3.1 (Optimal Value Function).** *If the admissible set of policies  $\pi(\mathbf{x}_{t+1:T}|\mathbf{x}_t)$  includes the auxiliary distribution  $\tilde{q}(\mathbf{x}_{t+1:T}|\mathbf{x}_t)$ , the optimal value function  $V_*^t(\mathbf{x}_t)$  (Equation (21)) satisfies:*

$$\tilde{q}(\mathbf{x}_t) = \frac{1}{Z} \exp(-V_*^t(\mathbf{x}_t)/\tau). \quad (15)$$

*Proof.* The result follows from the definition of the optimal value function and the theorem condition  $\min_{\pi} KL(\pi(\mathbf{x}_{t+1:T}|\mathbf{x}_t) \parallel \tilde{q}(\mathbf{x}_{t+1:T}|\mathbf{x}_t)) = 0$ . See Appendix B.1 for details.  $\square$

The second theorem provides a guideline for designing the auxiliary distribution  $\tilde{q}(\mathbf{x}_t)$ . The result shows that it is beneficial to choose an auxiliary distribution that transforms the target distribution into a Gaussian prior  $\pi(\mathbf{x}_0)$ . This choice is identical to how the forward process is designed in diffusion models (Sohl-Dickstein et al., 2015; Song et al., 2021).

**Theorem 3.2 (Optimal Auxiliary Distribution).** *Under the same assumptions as Theorem 3.1, the minimum value of our joint KL divergence objective is related to  $\tilde{q}(\mathbf{x}_0)$  as follows:*

$$\min_{\pi} KL(\pi(\mathbf{x}_{0:T}) \parallel \tilde{q}(\mathbf{x}_{0:T})) = KL(\pi(\mathbf{x}_0) \parallel \tilde{q}(\mathbf{x}_0)). \quad (16)$$

*Therefore, to fully minimize the objective to zero, the auxiliary distribution  $\tilde{q}(\mathbf{x}_{0:T-1}|\mathbf{x}_T)$  must satisfy:*

$$\tilde{q}(\mathbf{x}_0) = \pi(\mathbf{x}_0). \quad (17)$$

*Proof.* Using the definition of the optimal value function and the result from Theorem 3.1, we obtain:

$$\begin{aligned} & \min_{\pi} KL(\pi(\mathbf{x}_{0:T}) \parallel \tilde{q}(\mathbf{x}_{0:T})) \\ &= \mathbb{E}_{\pi(\mathbf{x}_0)} [\log \pi(\mathbf{x}_0) + V_*^0(\mathbf{x}_0)/\tau + \log Z] \\ &= KL(\pi(\mathbf{x}_0) \parallel \tilde{q}(\mathbf{x}_0)). \end{aligned} \quad \square$$

## 4. Sampling $n$ -Body Systems with VGS

Building on the general sampling problem discussed in the previous section, we now focus on the sampling problem under symmetry constraints. We demonstrate that VGS can effectively leverage the symmetry of the  $n$ -body system.

**Sampling the Equilibrium State of  $n$ -Body Systems** Sampling  $n$ -body systems is a fundamental problem with various real-world applications (Jumper et al., 2021; Hoogenboom et al., 2022). We represent the configuration of an

$n$ -body system in  $\mathbb{R}^m$  as  $\mathbf{x} \in \mathbb{R}^{n \times m}$ . Since the choice of the reference frame is arbitrary, the energy of the system,  $E(\mathbf{x})$ , must remain invariant under translations, rotations, and reflections of the particles. Furthermore, we assume that the particles are indistinguishable, which introduces permutation invariance. Taken together, the energy function  $E(\mathbf{x})$  must exhibit  $E(m) \times \mathbb{S}_n$ -invariance under the trivial group action—that is, transformations by  $E(m)$  and the permutations of the particles. Recent studies in training neural samplers have incorporated the symmetry of  $n$ -body systems into their algorithms, achieving state-of-the-art performance (Akhound-Sadegh et al., 2024; He et al., 2024).

**Incorporating Symmetries in VGS** We can leverage the symmetry of  $n$ -body systems by reducing the effective dimension from  $D = nm$  to  $D = (n-1)m$  and utilizing an  $E(m) \times \mathbb{S}_m$ -invariant value network with  $\alpha_t = 1$ .

The reduction in effective dimension arises from the fact that the system is translation-invariant, allowing us to project the set of particles onto a subspace that satisfies the zero-mean condition, i.e.,  $\mathcal{X} = \{\mathbf{x} \in \mathbb{R}^{n \times m} \mid \sum_{i=1}^n x_i = 0\}$ . This projection ensures that the Boltzmann distribution is well-defined on  $\mathcal{X}$ , as it is impossible to construct a translation-invariant measure on  $\mathbb{R}^{n \times m}$ . Consequently, we consider the case where  $\mu_{\phi}^t$  and  $\epsilon_t$  in Equation (3) are restricted to  $\mathcal{X}$ . Since  $\mathcal{X}$  is defined by  $m$  linear constraints, it is isomorphic to  $\mathbb{R}^{(n-1)m}$ . Therefore, the arguments in Section 3.2 remain valid while accounting for the reduced effective dimension.

We use an  $E(m) \times \mathbb{S}_n$ -invariant value network to reflect the invariance of the value function. The following theorem shows that, with  $\alpha_t = 1$ , the value function of VGS retains  $O(m) \times \mathbb{S}_n$ -invariance on  $\mathcal{X}$ .

**Theorem 4.1 (Invariance of the Value Function).** *Assume that the energy function is  $O(m) \times \mathbb{S}_n$ -invariant under the trivial group action  $\circ$ , as follows:*

$$E(g \circ \mathbf{x}) = E(\mathbf{x}) \quad \forall \mathbf{x} \in \mathcal{X}, g \in O(m) \times \mathbb{S}_n. \quad (18)$$

*If  $\alpha_t = 1$ , then the value function  $V_{\pi}^t$  of VGS preserves  $O(m) \times \mathbb{S}_n$ -invariance:*

$$V_{\pi}^t(g \circ \mathbf{x}_t) = V_{\pi}^t(\mathbf{x}_t) \quad \forall \mathbf{x}_t \in \mathcal{X}, g \in O(m) \times \mathbb{S}_n. \quad (19)$$

*Proof.* The proof follows by mathematical induction from  $t = T-1$  to  $t = 0$ . At each step, the fact that the gradient of a  $G$ -invariant function  $f: \mathcal{X} \rightarrow \mathbb{R}$  is  $G$ -equivariant is used, provided that  $G$  acts orthogonally on  $\mathcal{X}$  (Papamakarios et al., 2021, Lemma 2). For details, see Appendix B.2.  $\square$

Instead of projecting samples onto  $\mathcal{X}$  and applying an  $O(m) \times \mathbb{S}_n$ -invariant transformation, we directly use an  $E(m) \times \mathbb{S}_n$ -invariant value network. The invariant network is designed using the pairwise distances of particles as inputs (for details, see Section 7.2). Our approach is simpler than

**Algorithm 3** Training EBM with VGS

---

**Input:** EBM  $E_\theta(\mathbf{x})$ , Values  $V_\phi^t(\mathbf{x}_t)$ , Dataset  $\mathcal{D} = \{\mathbf{x}_i\}_{i=1}^N$ , Hyperparameter  $\gamma > 0$ , Regularizer functional  $Reg_\theta$ .

**for** each minibatch  $\mathbf{x}_i \sim \mathcal{D}$  **do**

Sample  $\mathbf{x}^- \sim \pi_\phi(\mathbf{x})$  by Algorithm 1

$\min_\theta E_\theta(\mathbf{x}_i) - E_\theta(\mathbf{x}^-) + \gamma Reg_\theta(\mathbf{x}_i, \mathbf{x}^-)$

Update  $V_\phi^t$  using Algorithm 2.

**end for**

---

constructing an equivariant network, as done in prior works (Akhound-Sadegh et al., 2024; He et al., 2024). Equivariant networks often rely on graph structures (Satorras et al., 2021) or require complex components such as spherical harmonics (Fuchs et al., 2020; Thomas et al., 2018).

## 5. Training Energy-Based Models with Value Gradient Samplers

This section describes how VGS can serve as an effective alternative to MCMC for EBM training.

**MCMC in EBM Training.** An EBM has the same form as the target density considered in Equation (1) but with the energy function  $E_\theta(\mathbf{x})$  having a trainable parameter  $\theta$ , i.e.,  $q_\theta(\mathbf{x}) = \frac{1}{Z_\theta} \exp(-E_\theta(\mathbf{x})/\tau)$ . Training an EBM amounts to finding  $\theta$  that makes  $q_\theta(\mathbf{x})$  as close as possible to the data generating density  $p(\mathbf{x})$  given only access to a set of training data  $\{\mathbf{x}_i\}_{i=1}^N \sim p(\mathbf{x})$ . Due to the intractable  $Z_\theta$ , evaluating the likelihood gradient requires sampling from model  $q_\theta(\mathbf{x})$  (Hinton, 2002):

$$\nabla_\theta \log q_\theta(\mathbf{x}) = -\nabla_\theta E_\theta(\mathbf{x}) + \mathbb{E}_{\mathbf{x}^- \sim q_\theta} [\nabla_\theta E_\theta(\mathbf{x}^-)],$$

where  $\mathbf{x}^-$  is often called “negative samples.” The EBM update usually involves a regularizer  $Reg_\theta(\mathbf{x}_i, \mathbf{x}^-)$  for the energy. The negative sample  $\mathbf{x}^- \sim q_\theta(\mathbf{x})$  is simulated by MCMC, which has been the key bottleneck in EBM training regarding computational efficiency and stability. Still, many implementations of deep EBMs use MCMC, such as Langevin Monte Carlo, to generate negative samples (Du & Mordatch, 2019; Gao et al., 2021; Yoon et al., 2021; 2023).

**Training EBMs with VGS.** Having a trainable neural sampler  $\pi_\phi(\mathbf{x})$  to replace MCMC has been shown to greatly stabilize training and often produce a more accurate energy function (Abbasnejad et al., 2019; Dai et al., 2019; 2017; Han et al., 2020; Kumar et al., 2019; Geng et al., 2021; 2024; Yoon et al., 2024). Many of the frameworks for incorporating  $\pi_\phi(\mathbf{x})$  have an equivalent objective function, which can be succinctly written as the following:

$$\min_\theta \max_\phi KL(p(\mathbf{x})||q_\theta(\mathbf{x})) - KL(\pi_\phi(\mathbf{x})||q_\theta(\mathbf{x})). \quad (20)$$

This minimax problem has the Nash equilibrium of

$p(\mathbf{x}) = q_\theta(\mathbf{x}) = \pi_\phi(\mathbf{x})$  when the models are well-specified. In practice, the equilibrium can be found by updating EBM  $q_\theta(\mathbf{x})$  and sampler  $\pi_\phi(\mathbf{x})$  alternately.

Being an algorithm aiming to (approximately) solve  $\min_\phi KL(\pi_\phi(\mathbf{x})||q_\theta(\mathbf{x}))$ , VGS can be used as a drop-in replacement for  $\pi_\phi(\mathbf{x})$  in Equation (20). Although VGS minimizes only the upper bound of the KL divergence, it shows promising empirical results. The process of training EBM using VGS is described in Algorithm 3.

## 6. Related Work

SDE-based samplers, such as PIS (Zhang & Chen, 2022), DIS (Berner et al., 2022), DDS (Vargas et al., 2023), and Richter & Berner (2024), inherently possess rich interpretation to the optimal control problem. Although discussed theoretically, the connection to optimal control is rarely exploited directly.

Sequentially drawing intermediate samples from a series of distributions that interpolate between the initial and target distributions is a recurring strategy in sampling. Classical sampling methods, such as SMC (Del Moral et al., 2006) and AIS (Neal, 2001), generate intermediate samples from tempered distributions. More recent works explore the use of diffused target densities as intermediate distributions. However, a key challenge in this setting is that the score of diffused densities cannot be estimated using the same techniques in diffusion modeling (Sohl-Dickstein et al., 2015; Ho et al., 2020; Song et al., 2021). To address this, various approaches have been proposed, leveraging different mathematical formulations (Akhound-Sadegh et al., 2024; Phillips et al., 2024; Huang et al., 2024; McDonald & Barron, 2022; Wang et al., 2024; Chen et al., 2024). VGS addresses the same challenge but with the toolbox of RL, as the value function is theoretically linked to the log of the diffused target density.

## 7. Experiments

### 7.1. Sampling from Synthetic Distributions

**Target Distributions.** We use two distributions as our sampling benchmarks: a 9-component Gaussian Mixture Model (GMM) illustrated in Figure 1. and a funnel distribution. Further details in Appendix E.1.

These benchmarks are chosen to demonstrate that our VGS produces results that are competitive with the baseline methods: PIS (Zhang & Chen, 2022), DIS (Berner et al., 2022), DDS (Vargas et al., 2023).

**Performance Metrics.** The comparisons are made based on three metrics: the Sinkhorn Distance ( $\mathcal{W}_\gamma^2 \downarrow$ ), the total variation distance-energy (TVD-E  $\downarrow$ ), and the error in esti-

Table 1. Sampler performance benchmark for GMM ( $d = 2$ ) and Funnel ( $d = 10$ ). The reported metrics are the mean and standard deviation over five trials.

	$T \downarrow$	$\mathcal{W}_\gamma^2 \downarrow$	TVD-E $\downarrow$	$\Delta \text{std} \downarrow$
<b>GMM (<math>d = 2</math>)</b>				
DiKL	1	0.033 $\pm$ 0.001	0.320 $\pm$ 0.002	0.052 $\pm$ 0.000
iDEM	1000	0.036 $\pm$ 0.001	0.412 $\pm$ 0.005	1.377 $\pm$ 0.014
PIS	200	0.302 $\pm$ 0.158	0.016 $\pm$ 0.001	1.968 $\pm$ 0.378
DIS	200	0.054 $\pm$ 0.002	0.017 $\pm$ 0.002	2.400 $\pm$ 0.045
DDS	256	0.049 $\pm$ 0.003	<b>0.015</b> $\pm$ 0.001	2.273 $\pm$ 0.102
VGS (Ours)	10	<b>0.021</b> $\pm$ 0.000	0.051 $\pm$ 0.002	0.062 $\pm$ 0.041
	20	<b>0.021</b> $\pm$ 0.001	0.062 $\pm$ 0.004	<b>0.024</b> $\pm$ 0.008
<b>Funnel (<math>d = 10</math>)</b>				
PIS	200	7.968 $\pm$ 0.610	0.248 $\pm$ 0.015	5.363 $\pm$ 0.124
DIS	200	7.834 $\pm$ 0.739	<b>0.245</b> $\pm$ 0.012	5.174 $\pm$ 0.158
DDS	256	7.489 $\pm$ 0.448	0.256 $\pm$ 0.015	6.495 $\pm$ 0.230
VGS (Ours)	10	7.616 $\pm$ 0.556	0.618 $\pm$ 0.018	7.929 $\pm$ 0.056
	30	<b>7.272</b> $\pm$ 0.674	0.377 $\pm$ 0.053	<b>5.059</b> $\pm$ 0.104

inating the average standard deviation across the marginal distributions ( $\Delta \text{std} \downarrow$ ). We also report the number of time steps to generate a sample ( $T$ ). Further details in Appendix E.2.

We report both  $\mathcal{W}_\gamma^2$  and TVD-E metrics to complement each other.  $\mathcal{W}_\gamma^2$  is less sensitive to noisy samples, whereas TVD-E is less sensitive to missing modes (He et al., 2024).

**VGS Implementation.** The trainable value function of the VGS sampler  $V_\phi^t : \mathbb{R}^d \times \mathbb{Z}^+ \rightarrow \mathbb{R}$  can be trained using any neural network architecture that incorporates time step embedding. We use a Fourier MLP architecture, an MLP with sinusoidal time step embedding. Further details in Appendix E.3.

**Results.** Table 1 demonstrates that VGS outperforms all baseline models across both target distributions, GMM and funnel. VGS achieved similar or superior performance compared to SDE-based samplers on  $\mathcal{W}_\gamma^2$  and  $\Delta \text{std}$  while using a significantly smaller number of time steps  $T$ .

**Effect of the Number of Time Steps.** We report the Sinkhorn distance  $\mathcal{W}_\gamma^2$  to the number of time steps  $T$  in GMM for our method and the baselines in Figure 2. Our method shows smaller  $\mathcal{W}_\gamma^2$  compared to DDS for all  $T$  under 100. We also proved that the performance of VGS is robust to  $T$ , while baselines such as DDS show a clear decline in performance when  $T$  is reduced due to their formulation in the continuous-time domain. Lastly, we proved that VGS’s performance on large numbers of  $T$  can be reproduced for small numbers of  $T$  by scaling noise.

**Training and Sampling Time.** We report the training and sampling times of VGS and baseline models for synthetic distributions in Table 4. Given the comparable model size, VGS shows faster training and sampling time than all

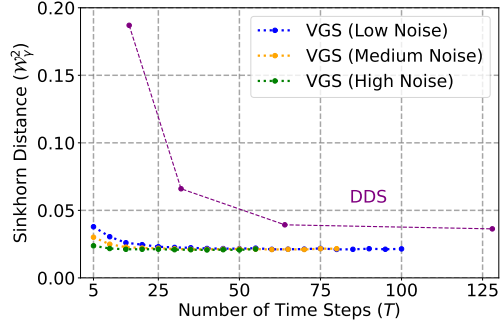


Figure 2. Sinkhorn distance  $\mathcal{W}_\gamma^2$  to the number of time steps  $T$  on GMM. Performance of VGS shows robustness to the number of time steps  $T$  and outperforms DDS on every  $T < 100$ . Increasing the noise magnitude  $s_t$  in VGS improves performance in the small  $T$  regime but makes training divergent when  $T$  is large.

SDE-based samplers (e.g., PIS, DIS, and DDS). Although each VGS step is more expensive than a step of SDE, as computing the gradient is usually more expensive than a forward pass, VGS supports a significantly smaller number of time steps to be faster than SDE samplers. Details can be found in Appendix E.4.

## 7.2. Sampling $n$ -Body Particle Systems

**Target Distributions.** We conduct experiments on two benchmark particle systems: a 4-particle double-well potential (DW-4) and a 13-particle Lennard-Jones potential (LJ-13). Both tasks were introduced in (Köhler et al., 2020) to evaluate sampler performance under invariant target distributions. Further details about the potentials are provided in Appendix E.1.

**Performance Metrics.** We evaluate performance using three metrics: the total variation distance of energy (TVD-E  $\downarrow$ ), the total variation distance of interatomic distances (TVD-D  $\downarrow$ ), and the Wasserstein-2 distance ( $\mathcal{W}^2 \downarrow$ ) between the test and generated samples. The samples are normalized to zero mean when computing  $\mathcal{W}^2$ . Since small changes in particle positions can lead to significant energy variations,  $\mathcal{W}^2$  may be a less meaningful metric in this experiment.

**Invariant Value Network.** We leverage the symmetry of particle systems by using  $E(m) \times \mathbb{S}_n$ -invariant value networks. To ensure  $E(m)$ -invariance, we use the  $n(n-1)/2$  pairwise distances of the particle system as inputs. This design is naturally invariant and retains all information, as the configuration of particles  $\mathbf{x}$  contains equivalent information to the pairwise distances (Satorras et al., 2021, Appendix E). Additionally, we sort the pairwise distances in descending order to further enforce  $\mathbb{S}_n$ -invariance.

**Results.** We compare the performance of VGS in sampling particle systems with state-of-the-art methods: FAB (Midgley et al., 2023), iDEM (Akhound-Sadegh et al.,

Table 2. Results of the  $n$ -body systems experiment. Baseline results are referenced from (He et al., 2024), and we report our results using the same evaluation process. For details, see Appendix E.3.2.

	TVD-E ↓	TVD-D ↓	$\mathcal{W}^2$ ↓
<b>DW-4</b> ( $d = 8$ )			
FAB	0.224±0.008	0.097±0.005	<b>1.554</b> ±0.015
iDEM	0.197±0.010	0.103±0.005	1.593±0.012
DiKL	0.162±0.016	0.146±0.006	1.579±0.019
VGS ( $T = 30$ )	<b>0.066</b> ±0.009	<b>0.057</b> ±0.004	1.610±0.027
<b>LJ-13</b> ( $d = 39$ )			
FAB	0.902±0.010	0.252±0.002	4.938±0.009
iDEM	0.306±0.013	0.044±0.001	4.172±0.007
DiKL	0.284±0.011	0.046±0.002	4.233±0.006
VGS ( $T = 100$ )	<b>0.112</b> ±0.009	<b>0.014</b> ±0.002	<b>4.167</b> ±0.005

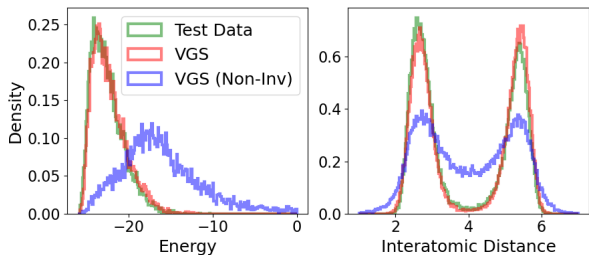


Figure 3. Energy (Left) and Interatomic Distance (Right) histograms of DW-4 samples from test data, VGS, and VGS with a non-invariant network. VGS generates accurate samples by leveraging the symmetry of the system.

2024), and DiKL (He et al., 2024). The results are summarized in Table 2. VGS outperforms other baseline methods based on the TVD-E and TVD-D metrics. We visualize the energy and interatomic distance histograms for DW-4 in Figure 3. As described in Section 4, we set  $D = (n - 1)m$  and  $\alpha_t = 1$  for all experiments. More experimental details are provided in Appendix E.3.2.

### 7.3. Training Energy-Based Models

#### 7.3.1. SYNTHETIC DISTRIBUTION

We train an EBM using VGS with  $T = 10$  following Algorithm 3 on a 2D 8 Gaussians dataset. For comparison, another EBM is trained using Langevin Monte Carlo with the same number of time steps as VGS. The squared energy regularizer is used:  $Reg_\theta(\mathbf{x}_i, \mathbf{x}^-) = E_\theta(\mathbf{x}_i)^2 + E_\theta(\mathbf{x}^-)^2$ . As shown in Figure 4, VGS recovers the accurate boundaries of the distributions and generates high-quality samples. Meanwhile, the EBM trained with Langevin Monte Carlo fails to reflect the true energy, even though Langevin Monte Carlo has the same mathematical form as VGS (Equation (3)). Note that short-run MCMC is known to produce inaccurate energy estimates in EBM training (Nijkamp et al., 2019; 2022), although it may generate feasible samples.

Table 3. Anomaly detection (DET) and localization (LOC) on MVTEC-AD. AUROC averaged over object categories is shown.

Model	DET	LOC
DRAEM (Zavrtanik et al., 2021)	88.1	87.2
MPDR (Yoon et al., 2023)	96.0	96.7
UniAD (You et al., 2022)	96.5±0.08	96.8±0.02
EBM+VGS (Ours)	<b>97.0</b> ±0.09	<b>97.1</b> ±0.01

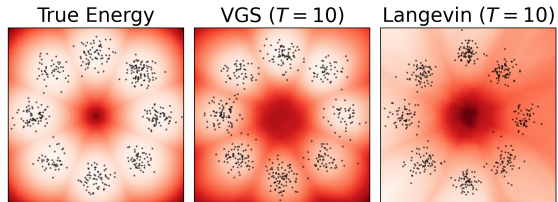


Figure 4. EBM training on 2D 8 Gaussians. The red shade depicts the energy, and the dots are the samples. VGS produces an accurate energy estimate, while the short-run MCMC does not.

#### 7.3.2. ENERGY-BASED ANOMALY DETECTION

An energy function that accurately captures the data distribution can be used in unsupervised anomaly detection, as an anomaly will be assigned a high energy value. When applied to MVTEC-AD, an industrial anomaly detection dataset (Bergmann et al., 2021), the EBM trained with VGS outperforms MPDR (Yoon et al., 2023), an EBM trained with a sophisticated MCMC scheme, as well as UniAD (You et al., 2022), a non-EBM method. We adopt the unified multi-class setup in You et al. (2022), which treats 15 object categories as a single class, resulting in multi-modal data distribution. The training set only consists of the normal class, and the test set contains the normal and the defective classes. All images are encoded into  $272 \times 14 \times 14$  vectors using EfficientNet-b4 (Tan & Le, 2019). The energy function is defined on the 272-dimensional space and applied across the spatial dimensions. The dataset supports detection and localization tasks, where the performance is measured by area under the receiver operating characteristic curve (AUROC) computed image-wise and pixel-wise, respectively. The summarized results are presented in Table 3. The full result and experimental details are in Appendix E.5.1.

## 8. Conclusion

This paper has formulated the sampling problem as a discrete-time continuous-space sequential decision-making problem. This fresh perspective allows us to employ the techniques from RL, which was previously considered disjoint from the statistical sampling problem. We believe this connection is still in its early stages of exploration and has the potential to inspire the development of new algorithms through the synergy of RL and statistical machine learning.



**Limitations.** First, VGS cannot generate samples in a single step. However, applying existing diffusion distillation techniques to VGS could potentially enable single-step sampling. Second, VGS does not provide an exact likelihood estimation for the generated samples, which prevents the direct use of techniques such as importance sampling, which relies on precise likelihood values. Third, the error of VGS is not mathematically quantified. We leave rigorous mathematical analysis as future work.

## Impact Statement

This work presents a novel algorithm for addressing the statistical problem of sampling. While its societal impact is not immediately apparent, the algorithm’s applications may have indirect effects, including advancing natural sciences and potentially enhancing malicious generative models. However, we do not identify any specific potential impacts requiring further discussion at this time.

## References

- Abbasnejad, M. E., Shi, Q., Hengel, A. v. d., and Liu, L. A generative adversarial density estimator. In *Proceedings of the IEEE/CVF Conference on Computer Vision and Pattern Recognition (CVPR)*, June 2019.
- Akhound-Sadegh, T., Rector-Brooks, J., Bose, J., Mittal, S., Lemos, P., Liu, C.-H., Sendera, M., Ravanbakhsh, S., Gidel, G., Bengio, Y., Malkin, N., and Tong, A. Iterated denoising energy matching for sampling from boltzmann densities. In *Forty-first International Conference on Machine Learning*, 2024. URL <https://openreview.net/forum?id=gVjMwLDFoQ>.
- Bergmann, P., Batzner, K., Fauser, M., Sattlegger, D., and Steger, C. The mvtec anomaly detection dataset: a comprehensive real-world dataset for unsupervised anomaly detection. *International Journal of Computer Vision*, 129(4):1038–1059, 2021.
- Berner, J., Richter, L., and Ullrich, K. An optimal control perspective on diffusion-based generative modeling. *arXiv preprint arXiv:2211.01364*, 2022.
- Chen, J., Richter, L., Berner, J., Blessing, D., Neumann, G., and Anandkumar, A. Sequential controlled langevin diffusions. *arXiv preprint arXiv:2412.07081*, 2024.
- Cuturi, M. Sinkhorn distances: Lightspeed computation of optimal transport. In Burges, C., Bottou, L., Welling, M., Ghahramani, Z., and Weinberger, K. (eds.), *Advances in Neural Information Processing Systems*, volume 26. Curran Associates, Inc., 2013. URL [https://proceedings.neurips.cc/paper\\_files/paper/2013/file/af21d0c97db2e27e13572cbf59eb343d-Paper.pdf](https://proceedings.neurips.cc/paper_files/paper/2013/file/af21d0c97db2e27e13572cbf59eb343d-Paper.pdf).
- Dai, B., Liu, Z., Dai, H., He, N., Gretton, A., Song, L., and Schuurmans, D. Exponential family estimation via adversarial dynamics embedding. In Wallach, H., Larochelle, H., Beygelzimer, A., d’Alché-Buc, F., Fox, E., and Garnett, R. (eds.), *Advances in Neural Information Processing Systems*, volume 32. Curran Associates, Inc., 2019. URL [https://proceedings.neurips.cc/paper\\_files/paper/2019/file/767d01b4bac1a1e8824c9b9f7cc79a04-Paper.pdf](https://proceedings.neurips.cc/paper_files/paper/2019/file/767d01b4bac1a1e8824c9b9f7cc79a04-Paper.pdf).
- Dai, Z., Almahairi, A., Bachman, P., Hovy, E., and Courville, A. Calibrating energy-based generative adversarial networks. In *International Conference on Learning Representations*, 2017. URL <https://openreview.net/forum?id=Syxeqhp911>.
- Del Moral, P., Doucet, A., and Jasra, A. Sequential monte carlo samplers. *Journal of the Royal Statistical Society Series B: Statistical Methodology*, 68(3):411–436, 05 2006. ISSN 1369-7412. doi: 10.1111/j.1467-9868.2006.00553.x. URL <https://doi.org/10.1111/j.1467-9868.2006.00553.x>.
- Du, Y. and Mordatch, I. Implicit generation and modeling with energy based models. In Wallach, H., Larochelle, H., Beygelzimer, A., d’Alché-Buc, F., Fox, E., and Garnett, R. (eds.), *Advances in Neural Information Processing Systems 32*, pp. 3608–3618. Curran Associates, Inc., 2019.
- Fuchs, F., Worrall, D., Fischer, V., and Welling, M. Se (3)-transformers: 3d roto-translation equivariant attention networks. *Advances in neural information processing systems*, 33:1970–1981, 2020.
- Gao, R., Song, Y., Poole, B., Wu, Y. N., and Kingma, D. P. Learning energy-based models by diffusion recovery likelihood. In *International Conference on Learning Representations*, 2021. URL [https://openreview.net/forum?id=v\\_1Soh8QUNc](https://openreview.net/forum?id=v_1Soh8QUNc).
- Geng, C., Wang, J., Gao, Z., Frellsen, J., and Hauberg, S. r. Bounds all around: training energy-based models with bidirectional bounds. In Ranzato, M., Beygelzimer, A., Dauphin, Y., Liang, P., and Vaughan, J. W. (eds.), *Advances in Neural Information Processing Systems*, volume 34, pp. 19808–19821. Curran Associates, Inc., 2021. URL [https://proceedings.neurips.cc/paper\\_files/paper/2021/file/a4d8e2a7e0d0c102339f97716d2fdfb6-Paper.pdf](https://proceedings.neurips.cc/paper_files/paper/2021/file/a4d8e2a7e0d0c102339f97716d2fdfb6-Paper.pdf).
- Geng, C., Han, T., Jiang, P.-T., Zhang, H., Chen, J., Hauberg, S., and Li, B. Improving adversarial energy-based model

- via diffusion process. *arXiv preprint arXiv:2403.01666*, 2024.
- Han, T., Nijkamp, E., Zhou, L., Pang, B., Zhu, S.-C., and Wu, Y. N. Joint training of variational auto-encoder and latent energy-based model. In *Proceedings of the IEEE/CVF Conference on Computer Vision and Pattern Recognition (CVPR)*, June 2020.
- He, J., Chen, W., Zhang, M., Barber, D., and Hernández-Lobato, J. M. Training neural samplers with reverse diffusive kl divergence. *arXiv preprint arXiv:2410.12456*, 2024.
- Heimel, T., Winterhalder, R., Butter, A., Isaacson, J., Krause, C., Maltoni, F., Mattelaer, O., and Plehn, T. MadNIS - Neural multi-channel importance sampling. *SciPost Phys.*, 15:141, 2023. doi: 10.21468/SciPostPhys.15.4.141. URL <https://scipost.org/10.21468/SciPostPhys.15.4.141>.
- Hinton, G. E. Training products of experts by minimizing contrastive divergence. *Neural computation*, 14(8):1771–1800, 2002.
- Ho, J., Jain, A., and Abbeel, P. Denoising diffusion probabilistic models. In Larochelle, H., Ranzato, M., Hadsell, R., Balcan, M., and Lin, H. (eds.), *Advances in Neural Information Processing Systems*, volume 33, pp. 6840–6851. Curran Associates, Inc., 2020. URL [https://proceedings.neurips.cc/paper\\_files/paper/2020/file/4c5bcfec8584af0d967f1ab10179ca4b-Paper.pdf](https://proceedings.neurips.cc/paper_files/paper/2020/file/4c5bcfec8584af0d967f1ab10179ca4b-Paper.pdf).
- Hoogeboom, E., Satorras, V. G., Vignac, C., and Welling, M. Equivariant diffusion for molecule generation in 3d. In *International conference on machine learning*, pp. 8867–8887. PMLR, 2022.
- Huang, X., Dong, H., HAO, Y., Ma, Y., and Zhang, T. Reverse diffusion monte carlo. In *The Twelfth International Conference on Learning Representations*, 2024. URL <https://openreview.net/forum?id=kIPEyMSdFV>.
- Jumper, J., Evans, R., Pritzel, A., Green, T., Figurnov, M., Ronneberger, O., Tunyasuvunakool, K., Bates, R., Žídek, A., Potapenko, A., et al. Highly accurate protein structure prediction with alphafold. *nature*, 596(7873):583–589, 2021.
- Kidger, P., Foster, J., Li, X., and Lyons, T. J. Neural sdes as infinite-dimensional gans. In Meila, M. and Zhang, T. (eds.), *Proceedings of the 38th International Conference on Machine Learning*, volume 139 of *Proceedings of Machine Learning Research*, pp. 5453–5463. PMLR, 18–24 Jul 2021a. URL <https://proceedings.mlr.press/v139/kidger21b.html>.
- Kidger, P., Foster, J., Li, X. C., and Lyons, T. Efficient and accurate gradients for neural sdes. In Ranzato, M., Beygelzimer, A., Dauphin, Y., Liang, P., and Vaughan, J. W. (eds.), *Advances in Neural Information Processing Systems*, volume 34, pp. 18747–18761. Curran Associates, Inc., 2021b. URL [https://proceedings.neurips.cc/paper\\_files/paper/2021/file/9ba196c7a6e89eafd0954de80fclb224-Paper.pdf](https://proceedings.neurips.cc/paper_files/paper/2021/file/9ba196c7a6e89eafd0954de80fclb224-Paper.pdf).
- Köhler, J., Klein, L., and Noé, F. Equivariant flows: Exact likelihood generative learning for symmetric densities, 2020. URL <https://arxiv.org/abs/2006.02425>.
- Kumar, R., Ozair, S., Goyal, A., Courville, A., and Bengio, Y. Maximum entropy generators for energy-based models. *arXiv preprint arXiv:1901.08508*, 2019.
- Leimkuhler, B. and Matthews, C. *Molecular Dynamics: With Deterministic and Stochastic Numerical Methods*. Springer, Cham, Switzerland, 2015. ISBN 978-3-319-16374-1. doi: 10.1007/978-3-319-16375-8. URL <https://link.springer.com/book/10.1007/978-3-319-16375-8>.
- Lin, L.-J. Self-improving reactive agents based on reinforcement learning, planning and teaching. *Machine Learning*, 8:293–321, 1992.
- McDonald, C. and Barron, A. Proposal of a score based approach to sampling using monte carlo estimation of score and oracle access to target density. *arXiv preprint arXiv:2212.03325*, 2022.
- Midgley, L. I., Stimper, V., Simm, G. N. C., Schölkopf, B., and Hernández-Lobato, J. M. Flow annealed importance sampling bootstrap. In *The Eleventh International Conference on Learning Representations*, 2023. URL <https://openreview.net/forum?id=XCTVFJws9LJ>.
- Mnih, V., Kavukcuoglu, K., Silver, D., Rusu, A. A., Veness, J., Bellemare, M. G., Graves, A., Riedmiller, M., Fidjeland, A. K., Ostrovski, G., et al. Human-level control through deep reinforcement learning. *nature*, 518(7540): 529–533, 2015.
- Neal, R. M. Annealed importance sampling. *Statistics and computing*, 11:125–139, 2001.
- Neal, R. M. Slice sampling. *the annals of statistics. Project Euclid*, 2003. URL <https://doi.org/10.1214/aos/1056562461>.

- Nijkamp, E., Hill, M., Zhu, S.-C., and Wu, Y. N. Learning non-convergent non-persistent short-run mcmc toward energy-based model. In Wallach, H., Larochelle, H., Beygelzimer, A., d'Alché-Buc, F., Fox, E., and Garnett, R. (eds.), *Advances in Neural Information Processing Systems*, volume 32, pp. 5232–5242. Curran Associates, Inc., 2019. URL <https://proceedings.neurips.cc/paper/2019/file/2bc8ae25856bc2a6a1333d1331a3b7a6-Paper.pdf>.
- Nijkamp, E., Gao, R., Sountsov, P., Vasudevan, S., Pang, B., Zhu, S.-C., and Wu, Y. N. MCMC should mix: Learning energy-based model with neural transport latent space MCMC. In *International Conference on Learning Representations*, 2022. URL <https://openreview.net/forum?id=4C93Qvn-tz>.
- Noé, F., Olsson, S., Köhler, J., and Wu, H. Boltzmann generators: Sampling equilibrium states of many-body systems with deep learning. *Science*, 365(6457):eaaw1147, 2019. doi: 10.1126/science.aaw1147. URL <https://www.science.org/doi/abs/10.1126/science.aaw1147>.
- Papamakarios, G., Nalisnick, E., Rezende, D. J., Mohamed, S., and Lakshminarayanan, B. Normalizing flows for probabilistic modeling and inference. *Journal of Machine Learning Research*, 22(57):1–64, 2021.
- Phillips, A., Dau, H.-D., Hutchinson, M. J., Bortoli, V. D., Deligiannidis, G., and Doucet, A. Particle denoising diffusion sampler. In *Forty-first International Conference on Machine Learning*, 2024. URL <https://openreview.net/forum?id=vMUnnS4OWC>.
- Richter, L. and Berner, J. Improved sampling via learned diffusions. In *The Twelfth International Conference on Learning Representations*, 2024. URL <https://openreview.net/forum?id=h4pNROsO06>.
- Roberts, G. O., Tweedie, R. L., et al. Exponential convergence of langevin distributions and their discrete approximations. *Bernoulli*, 2(4):341–363, 1996.
- Satorras, V. G., Hoogeboom, E., and Welling, M. E (n) equivariant graph neural networks. In *International conference on machine learning*, pp. 9323–9332. PMLR, 2021.
- Sohl-Dickstein, J., Weiss, E., Maheswaranathan, N., and Ganguli, S. Deep unsupervised learning using nonequilibrium thermodynamics. In Bach, F. and Blei, D. (eds.), *Proceedings of the 32nd International Conference on Machine Learning*, volume 37 of *Proceedings of Machine Learning Research*, pp. 2256–2265, Lille, France, 07–09 Jul 2015. PMLR. URL <https://proceedings.mlr.press/v37/sohl-dickstein15.html>.
- Song, Y., Sohl-Dickstein, J., Kingma, D. P., Kumar, A., Ermon, S., and Poole, B. Score-based generative modeling through stochastic differential equations. In *International Conference on Learning Representations*, 2021. URL <https://openreview.net/forum?id=PxtTIG12RRHS>.
- Tan, M. and Le, Q. Efficientnet: Rethinking model scaling for convolutional neural networks. In *International conference on machine learning*, pp. 6105–6114. PMLR, 2019.
- Thomas, N., Smidt, T., Kearnes, S., Yang, L., Li, L., Kohlhoff, K., and Riley, P. Tensor field networks: Rotation-and translation-equivariant neural networks for 3d point clouds. *arXiv preprint arXiv:1802.08219*, 2018.
- Tzen, B. and Raginsky, M. Neural stochastic differential equations: Deep latent gaussian models in the diffusion limit. *arXiv preprint arXiv:1905.09883*, 2019.
- Vargas, F., Grathwohl, W. S., and Doucet, A. Denoising diffusion samplers. In *The Eleventh International Conference on Learning Representations*, 2023. URL <https://openreview.net/forum?id=8pvnfTABulf>.
- Wang, Y., Guo, L., Wu, H., and Zhou, T. Energy based diffusion generator for efficient sampling of boltzmann distributions. *arXiv preprint arXiv:2401.02080*, 2024.
- Yoon, S., Noh, Y.-K., and Park, F. Autoencoding under normalization constraints. In Meila, M. and Zhang, T. (eds.), *Proceedings of the 38th International Conference on Machine Learning*, volume 139 of *Proceedings of Machine Learning Research*, pp. 12087–12097. PMLR, 18–24 Jul 2021.
- Yoon, S., Jin, Y.-U., Noh, Y.-K., and Park, F. C. Energy-based models for anomaly detection: A manifold diffusion recovery approach. In *Thirty-seventh Conference on Neural Information Processing Systems*, 2023. URL <https://openreview.net/forum?id=4nSDDokpfK>.
- Yoon, S., Hwang, H., Kwon, D., Noh, Y.-K., and Park, F. C. Maximum entropy inverse reinforcement learning of diffusion models with energy-based models. In *The Thirty-eighth Annual Conference on Neural Information Processing Systems*, 2024. URL <https://openreview.net/forum?id=V0oJaLqY4E>.
- You, Z., Cui, L., Shen, Y., Yang, K., Lu, X., Zheng, Y., and Le, X. A unified model for multi-class anomaly detection. In Koyejo, S., Mohamed, S., Agarwal, A., Belgrave, D., Cho, K., and Oh, A. (eds.), *Advances in Neural Information Processing Systems*, volume 35, pp. 4571–4584. Curran Associates, Inc., 2022.

Zavrtanik, V., Kristan, M., and Skočaj, D. Draem - a discriminatively trained reconstruction embedding for surface anomaly detection. In *Proceedings of the IEEE/CVF International Conference on Computer Vision (ICCV)*, pp. 8330–8339, October 2021.

Zhang, Q. and Chen, Y. Path integral sampler: A stochastic control approach for sampling. In *International Conference on Learning Representations, 2022*. URL [https://openreview.net/forum?id=\\_uCb2ynRu7Y](https://openreview.net/forum?id=_uCb2ynRu7Y).

## A. Bellman Optimality Equation

The optimal value function  $V_*^t(\mathbf{x}_t)$  for our optimal control problem Equation (5) is defined as follows:

$$V_*^t(\mathbf{x}_t) = \min_{\pi} \mathbb{E}_{\pi} \left[ E(\mathbf{x}_T) + \tau \sum_{t'=t}^{T-1} \log \frac{\pi(\mathbf{x}_{t'+1}|\mathbf{x}_{t'})}{\tilde{q}(\mathbf{x}_{t'}|\mathbf{x}_{t'+1})} \middle| \mathbf{x}_t \right]. \quad (21)$$

Bellman optimality equation is given as follows:

$$V_*^t(\mathbf{x}_t) = \min_{\pi(\mathbf{x}_{t+1}|\mathbf{x}_t)} \mathbb{E}_{\pi(\mathbf{x}_{t+1}|\mathbf{x}_t)} \left[ V_*^{t+1}(\mathbf{x}_{t+1}) + \tau \log \frac{\pi(\mathbf{x}_{t+1}|\mathbf{x}_t)}{\tilde{q}(\mathbf{x}_t|\mathbf{x}_{t+1})} \middle| \mathbf{x}_t \right]. \quad (22)$$

## B. Proof of Theorems

### B.1. Proof of Theorem 3.1

**Theorem 3.1** (Optimal Value Function) If the admissible set of policies  $\pi(\mathbf{x}_{t+1:T}|\mathbf{x}_t)$  includes the auxiliary distribution  $\tilde{q}(\mathbf{x}_{t+1:T}|\mathbf{x}_t)$ , the optimal value function  $V_*^t(\mathbf{x}_t)$  (Equation (21)) satisfies:

$$\tilde{q}(\mathbf{x}_t) = \frac{1}{Z} \exp(-V_*^t(\mathbf{x}_t)/\tau). \quad (23)$$

*Proof.* By assumption,  $\min_{\pi} KL(\pi(\mathbf{x}_{t+1:T}|\mathbf{x}_t)|\tilde{q}(\mathbf{x}_{t+1:T}|\mathbf{x}_t)) = 0$ . Since KL divergence is always non-negative, this minimum is attained when  $\pi(\mathbf{x}_{t+1:T}|\mathbf{x}_t) = \tilde{q}(\mathbf{x}_{t+1:T}|\mathbf{x}_t)$ . From the definition of the optimal value function in Equation (21), we obtain:

$$\begin{aligned} V_*^t(\mathbf{x}_t) &= \min_{\pi} \mathbb{E}_{\pi} \left[ E(\mathbf{x}_T) + \tau \sum_{t'=t}^{T-1} \log \frac{\pi(\mathbf{x}_{t'+1}|\mathbf{x}_{t'})}{\tilde{q}(\mathbf{x}_{t'}|\mathbf{x}_{t'+1})} \middle| \mathbf{x}_t \right] \\ &= \min_{\pi} \tau \mathbb{E}_{\pi(\mathbf{x}_{t+1:T}|\mathbf{x}_t)} \left[ -\log \tilde{q}(\mathbf{x}_{t:T}) + \log \pi(\mathbf{x}_{t+1:T}|\mathbf{x}_t) \middle| \mathbf{x}_t \right] - \tau \log Z \\ &= \min_{\pi} \tau \mathbb{E}_{\pi(\mathbf{x}_{t+1:T}|\mathbf{x}_t)} \left[ -\log \tilde{q}(\mathbf{x}_{t+1:T}|\mathbf{x}_t) + \log \pi(\mathbf{x}_{t+1:T}|\mathbf{x}_t) \middle| \mathbf{x}_t \right] - \tau \log \tilde{q}(\mathbf{x}_t) - \tau \log Z \\ &= \min_{\pi} \tau KL(\pi(\mathbf{x}_{t+1:T}|\mathbf{x}_t)|\tilde{q}(\mathbf{x}_{t+1:T}|\mathbf{x}_t)) - \tau \log \tilde{q}(\mathbf{x}_t) - \tau \log Z \\ &= -\tau \log \tilde{q}(\mathbf{x}_t) - \tau \log Z. \end{aligned} \quad (24)$$

Here, we slightly abuse notation by writing  $\tilde{q}(\mathbf{x}_{t+1:T}) = \tilde{q}(\mathbf{x}_{t+1:T-1}|\mathbf{x}_T)q(\mathbf{x}_T)$  and  $\tilde{q}(\mathbf{x}_{t+1:T}|\mathbf{x}_t) = \tilde{q}(\mathbf{x}_{t+1:T-1}|\mathbf{x}_t, \mathbf{x}_T)q(\mathbf{x}_T)$ . Rearranging Equation (24), we obtain:

$$\tilde{q}(\mathbf{x}_t) = \frac{1}{Z} \exp(-V_*^t(\mathbf{x}_t)/\tau). \quad (25)$$

□

### B.2. Proof of Theorem 4.1

**Theorem 4.1** (Invariance of the Value Function) Assume that the energy function is  $O(m) \times \mathbb{S}_n$ -invariant under the trivial group action  $\circ$ , as follows:

$$E(g \circ \mathbf{x}) = E(\mathbf{x}) \quad \forall \mathbf{x} \in \mathcal{X}, g \in O(m) \times \mathbb{S}_n. \quad (26)$$

If  $\alpha_t = 1$ , then the value function  $V_{\pi}^t$  of VGS preserves  $O(m) \times \mathbb{S}_n$ -invariance:

$$V_{\pi}^t(g \circ \mathbf{x}_t) = V_{\pi}^t(\mathbf{x}_t) \quad \forall \mathbf{x}_t \in \mathcal{X}, g \in O(m) \times \mathbb{S}_n. \quad (27)$$

*Proof.* Substituting  $\alpha_t = 1$  and  $\mu_t(\mathbf{x}_t) = -\frac{s_t^2 \alpha_t^2}{\tau} \nabla_{\alpha_t \mathbf{x}_t} V_{\pi}^{t+1}(\alpha_t \mathbf{x}_t)$ ,  $\sigma_t = \alpha_t s_t$  into Equation (10), we derive the Bellman equation for VGS as follows:

$$V_{\pi}^t(\mathbf{x}_t) = \frac{s_t^2 \|\nabla_{\mathbf{x}_t} V_{\pi}^{t+1}(\mathbf{x}_t)\|^2}{2\tau} + \mathbb{E}_{\epsilon_t} [V_{\pi}^{t+1}(\mathbf{x}_t - \frac{s_t^2}{\tau} \nabla_{\mathbf{x}_t} V_{\pi}^{t+1}(\mathbf{x}_t) + s_t \epsilon_t)]. \quad (28)$$

Assuming that  $V_\pi^{t+1}$  is  $O(m) \times \mathbb{S}_n$ -invariant, we aim to show that  $V_\pi^t$  is also  $O(m) \times \mathbb{S}_n$ -invariant. Since  $\|g \circ \mathbf{x}\| = \|\mathbf{x}\|$  for all  $\mathbf{x} \in \mathcal{X}$ ,  $\circ$  is an orthogonal action. Therefore  $\nabla V_\pi^{t+1}$  is equivariant under this action, implying that  $\nabla_{g \circ \mathbf{x}_{t+1}} V_\pi^{t+1}(g \circ \mathbf{x}_{t+1}) = g \circ \nabla_{\mathbf{x}_{t+1}} V_\pi^{t+1}(\mathbf{x}_{t+1})$  (Papamakarios et al., 2021, Lemma 2). Using this property we obtain:

$$V_\pi^t(g \circ \mathbf{x}_t) = \frac{s_t^2 \|\nabla_{g \circ \mathbf{x}_t} V_\pi^{t+1}(g \circ \mathbf{x}_t)\|^2}{2\tau} + \mathbb{E}_{\epsilon_t} [V_\pi^{t+1}(g \circ \mathbf{x}_t - \frac{s_t^2}{\tau} \nabla_{g \circ \mathbf{x}_t} V_\pi^{t+1}(g \circ \mathbf{x}_t) + s_t \epsilon_t)] \quad (29)$$

$$= \frac{s_t^2 \|g \circ \nabla_{\mathbf{x}_t} V_\pi^{t+1}(\mathbf{x}_t)\|^2}{2\tau} + \mathbb{E}_{\epsilon_t} [V_\pi^{t+1}(g \circ (\mathbf{x}_t - \frac{s_t^2}{\tau} \nabla_{\mathbf{x}_t} V_\pi^{t+1}(\mathbf{x}_t) + s_t (g^{-1} \circ \epsilon_t)))] \quad (30)$$

$$= \frac{s_t^2 \|\nabla_{\mathbf{x}_t} V_\pi^{t+1}(\mathbf{x}_t)\|^2}{2\tau} + \mathbb{E}_{\epsilon'_t = g^{-1} \circ \epsilon_t} [V_\pi^{t+1}(g \circ (\mathbf{x}_t - \frac{s_t^2}{\tau} \nabla_{\mathbf{x}_t} V_\pi^{t+1}(\mathbf{x}_t) + s_t \epsilon'_t))] \quad (31)$$

$$= \frac{s_t^2 \|\nabla_{\mathbf{x}_t} V_\pi^{t+1}(\mathbf{x}_t)\|^2}{2\tau} + \mathbb{E}_{\epsilon_t} [V_\pi^{t+1}(\mathbf{x}_t - \frac{s_t^2}{\tau} \nabla_{\mathbf{x}_t} V_\pi^{t+1}(\mathbf{x}_t) + s_t \epsilon_t)] = V_\pi^t(\mathbf{x}_t). \quad (32)$$

For the final equality, we used the fact that the probability density function of a Gaussian random variable is  $O(m) \times \mathbb{S}_n$ -invariant, which implies  $\epsilon'_t \sim \mathcal{N}(0, I)$ .

The theorem result follows by mathematical induction, as  $V^T(\mathbf{x}_T) = E(\mathbf{x}_T)$  is  $O(n) \times S_m$ -invariant by the assumption of the theorem.  $\square$

### C. Detailed Derivation of VGS

In this section we present a detailed derivation process of a more accurate approximation of optimal drift and diffusion for VGS. We begin from the optimization problem of Equation (10). We apply second-order Taylor expansion of  $V_\pi^{t+1}$  with respect to  $\alpha_t \mathbf{x}_t$ .

$$\begin{aligned} & \mathbb{E}_\epsilon [V_\pi^{t+1}(\alpha_t \mathbf{x}_t + \mu_t + \sigma_t \epsilon)] \\ & \approx \mathbb{E}_\epsilon \left[ V_\pi^{t+1}(\alpha_t \mathbf{x}_t) + (\mu_t + \sigma_t \epsilon)^\top \nabla_{\alpha_t \mathbf{x}_t} V_\pi^{t+1}(\alpha_t \mathbf{x}_t) + \frac{1}{2} (\mu_t + \sigma_t \epsilon)^\top \nabla \nabla_{\alpha_t \mathbf{x}_t} V_\pi^{t+1}(\alpha_t \mathbf{x}_t) (\mu_t + \sigma_t \epsilon) \right] \\ & = V_\pi^{t+1}(\alpha_t \mathbf{x}_t) + \mu_t^\top \nabla_{\alpha_t \mathbf{x}_t} V_\pi^{t+1}(\alpha_t \mathbf{x}_t) + \frac{1}{2} \mu_t^\top \nabla \nabla_{\alpha_t \mathbf{x}_t} V_\pi^{t+1}(\alpha_t \mathbf{x}_t) \mu_t + \frac{1}{2} \sigma_t^2 \nabla_{\alpha_t \mathbf{x}_t}^2 V_\pi^{t+1}(\alpha_t \mathbf{x}_t). \end{aligned} \quad (33)$$

Substituting the approximation into Equation (10) and removing constant terms, we rewrite the optimization problem as follows:

$$\begin{aligned} & \min_{\mu_t, \sigma_t} V_\pi^{t+1}(\alpha_t \mathbf{x}_t) + \mu_t^\top \nabla_{\alpha_t \mathbf{x}_t} V_\pi^{t+1}(\alpha_t \mathbf{x}_t) + \frac{1}{2} \mu_t^\top \nabla \nabla_{\alpha_t \mathbf{x}_t} V_\pi^{t+1}(\alpha_t \mathbf{x}_t) \mu_t + \frac{1}{2} \sigma_t^2 \nabla_{\alpha_t \mathbf{x}_t}^2 V_\pi^{t+1}(\alpha_t \mathbf{x}_t) \\ & \quad - \tau D \log \sigma_t + \frac{\tau \|\mu_t\|^2}{2s_t^2 \alpha_t^2} + \frac{\tau D \sigma_t^2}{2s_t^2 \alpha_t^2}. \end{aligned} \quad (34)$$

Setting the derivatives of Equation (34) with respect to  $\mu_t$  and  $\sigma_t$  to zero, we derive the analytic expressions of the optimal drift  $\mu_t$  and optimal noise magnitude  $\sigma_t$  as follows:

VGS with first-order approximation:

$$\mu_t = -\frac{s_t^2 \alpha_t^2}{\tau} \nabla_{\alpha_t \mathbf{x}_t} V_\pi^{t+1}(\alpha_t \mathbf{x}_t), \quad \sigma_t = \alpha_t s_t. \quad (35)$$

VGS with second-order approximation:

$$\mu_t = -\left( \nabla \nabla_{\alpha_t \mathbf{x}_t} V_\pi^{t+1}(\alpha_t \mathbf{x}_t) + \frac{\tau}{\alpha_t^2 s_t^2} I \right)^{-1} \nabla_{\alpha_t \mathbf{x}_t} V_\pi^{t+1}(\alpha_t \mathbf{x}_t), \quad \sigma_t = \frac{\alpha_t s_t}{\sqrt{1 + \alpha_t^2 s_t^2 \nabla_{\alpha_t \mathbf{x}_t}^2 V_\pi^{t+1}(\alpha_t \mathbf{x}_t) / (\tau D)}}. \quad (36)$$

### D. Training the Initial Distribution

Along with the value function, we can jointly train the initial distribution of VGS by optimizing  $\sigma_{init}$ . We reformulate our joint KL divergence minimization objective (right-hand side of Equation (4)) with  $\sigma_{init}$  as an optimization variable:

$$\min_{\sigma_{init}} \mathbb{E}_{\pi_\phi(\mathbf{x}_{0:T})} \left[ E(\mathbf{x}_T) + \tau \sum_{t=0}^{T-1} \log \frac{\pi_\phi(\mathbf{x}_{t+1} | \mathbf{x}_t)}{\tilde{q}(\mathbf{x}_t | \mathbf{x}_{t+1})} + \tau \log \pi(\mathbf{x}_0) \right]. \quad (37)$$

Recall that  $\mathbf{x}_0 \sim \mathcal{N}(0, \sigma_{init}^2 I)$ , which implies that  $\mathbb{E}_{\pi_{\phi}(\mathbf{x}_0:T)}[\log \pi(\mathbf{x}_0)] = -D \log \sigma_{init} + \text{Const}$ . Using the definition of the value function, we simplify the optimization problem as follows:

$$\min_{\sigma_{init}} \mathbb{E}_{\pi(\mathbf{x}_0)}[V_{\pi}^0(\mathbf{x}_0) - \tau D \log \sigma_{init}]. \quad (38)$$

Thus, in our experiments, we update  $\sigma_{init}$  according to:

$$\min_{\sigma_{init}} \mathbb{E}_{z \sim \mathcal{N}(0, I)}[V_{\phi}^0(\sigma_{init} z) - \tau D \log \sigma_{init}]. \quad (39)$$

We set the initial value of  $\sigma_{init}$  as  $\sigma_{init}^2 = (1 + \sum_{t=0}^{T-1} s_t^2)$  when using the variance-exploding process for  $\tilde{q}(\mathbf{x}_t | \mathbf{x}_{t+1})$  and as  $\sigma_{init}^2 = 1$  when using the variance-preserving process for  $\tilde{q}(\mathbf{x}_t | \mathbf{x}_{t+1})$ . This choice is motivated by the result of Theorem 3.2, ensuring that  $\pi(\mathbf{x}_0) = \tilde{q}(\mathbf{x}_0)$  when  $q(\mathbf{x})$  is a unit Gaussian.

## E. Additional Details of Experiments

### E.1. Target Distributions

**GMM (Berner et al., 2022):** We use a 2-dimensional Gaussian Mixture Model, with its density given by  $\rho(x) = \frac{1}{m} \sum_{i=1}^m \mathcal{N}(x; \mu_i, \Sigma_i)$ , where  $m = 9$ ,  $(\mu_i)_{i=1}^9 = \{-5, 0, 5\} \times \{-5, 0, 5\} \subset \mathbb{R}^2$  and  $(\Sigma_i)_{i=1}^9 = 0.3\mathbf{I} \subset \mathbb{R}^{2 \times 2}$ . With these parameters, a 9-component Gaussian Mixture density with evenly separated modes is obtained. A well-trained sampler must be able to sample from all nine modes.

**Funnel (Neal, 2003):** We use a 10-dimensional funnel distribution with its density given by  $\rho(x) = \mathcal{N}(x_1; 0, \sigma^2) \prod_{i=1}^d \mathcal{N}(x_i; 0, e^{x_1})$ , where  $x \in \mathbb{R}^d$ . The specific parameters are  $d = 10$  and  $\sigma = 3$ . The funnel distribution is known to be a challenging distribution for testing MCMC methods, as the variance grows exponentially as the first dimension  $x_1$  increases.

**DW-4 (Köhler et al., 2020):** This system consists of 4 particles in 2-dimensions. Each pair of particles interacts via a *double well* potential  $u^{\text{DW}}(x) = \frac{1}{2\tau} \sum_{i,j} \left[ a(d_{ij} - d_0) + b(d_{ij} - d_0)^2 + c(d_{ij} - d_0)^4 \right]$ , where  $d_{ij}$  represents the pairwise distance between two particles  $i$  and  $j$ . These pairwise interactions produce multiple metastable states in the system. All parameters  $a, b, c, d_0$  and  $\tau$  are set to match those used in the experiment from DiKL(He et al., 2024).

**LJ-13 (Köhler et al., 2020):** We employ a system of 13 particles in 3-dimensions with the *Lennard-Jones* (LJ) potential  $u^{\text{LJ}}(x) = \frac{\epsilon}{2\tau} \left[ \sum_{i,j} \left( \left( \frac{r_m}{d_{ij}} \right)^{12} - 2 \left( \frac{r_m}{d_{ij}} \right)^6 \right) \right]$ , where  $d_{ij}$  represents the pairwise distance between two particles  $i$  and  $j$ . In this system, the energy landscape is highly complex, making it difficult to find the energy minima. Therefore, this system is considered good benchmark for evaluating structure generation methods. The parameters  $\epsilon, r_m$  and  $\tau$  are chosen to be the same as those used in the experiment from DiKL(He et al., 2024).

### E.2. Performance Metrics

**Total Variation Distance - Energy, (Interatomic) Distance (TVD-E, D):** The general Total Variation Distance (TVD) measures the difference between two distributions as  $\text{TVD}(P, Q) = \frac{1}{2} \int_{\mathcal{X}} |P(x) - Q(x)| dx$ . We compute a discrete approximation of TVD using histogram-based probability distributions, following DiKL(He et al., 2024). TVD-Energy (TVD-E) measures the difference between the energy distributions of the generated samples and the validation set, while TVD-Distance (TVD-D) quantifies the difference in interatomic distance distributions between particles.

**Error for Estimating the Average Standard Deviation Across the Marginals ( $\Delta \text{std}$ ):** We report the error for estimating the average standard deviation across the marginal, following the method proposed in (Richter & Berner, 2024). Given a learned distribution of the sampler  $p_{\text{sampler}}$  and a target distribution  $p_{\text{target}}$  with  $d$ -dimensional data, we compute the metric  $\Delta \text{std} = \frac{1}{d} \sum_{k=1}^d \left| \sqrt{\mathbb{V}[P_k]} - \sqrt{\mathbb{V}[G_k]} \right|$ , where  $P \sim p_{\text{sampler}}$  and  $G \sim p_{\text{target}}$ .

**Wasserstein-2 Distance ( $\mathcal{W}^2$ ):** The standard 2-Wasserstein distance between two distributions is defined as  $\mathcal{W}_2(P, Q) = \left( \inf_{\pi} \int \pi(x, y) d(x, y)^2 dx dy \right)^{\frac{1}{2}}$ , where  $\pi$  is the transport plan with marginals constrained to  $P$  and  $Q$  respectively (Akhound-Sadegh et al., 2024). We use the Euclidean distance  $\|x - y\|_2$  for  $d(x, y)$  and calculate the 2-Wasserstein distance between generated samples from the sampler and the ground truth data.

**Sinkhorn Distance** ( $\mathcal{W}_\gamma^2$ ): The Sinkhorn distance is a metric which approximates the optimal transport distance. It adds entropic regularization to the Wasserstein distance in solving optimal transport problem, which is aimed to penalize highly deterministic transport plans (Cuturi, 2013). It is defined as  $\mathcal{W}_\gamma^2(P, Q) = (\inf_\pi \int \pi(x, y) d(x, y)^2 dx dy + \gamma H(\pi))^{\frac{1}{2}}$  where  $\pi$  is the transport plan with marginals constrained to  $P$  and  $Q$ ,  $\gamma$  is a parameter to balance between the Wasserstein term and the entropy term, and  $H(\pi)$  is the entropy term of the  $\pi$ , given by  $H(\pi) = - \int \pi(x, y) \log(\pi(x, y)) dx dy$ . We utilize the Sinkhorn distance implementation in <https://github.com/fwilliams/scalable-pytorch-sinkhorn> for efficient computation.

### E.3. Experimental Details

#### E.3.1. SAMPLING FROM SYNTHETIC DISTRIBUTION EXPERIMENTS

For the synthetic distribution experiments, we conducted 5 independent runs with different seeds for each experiment. All reported metrics are the averages of the 5 runs, along with their standard deviation. Every experiment is performed on a single NVIDIA RTX 3090 (24GB) GPU.

**GMM:** VGS uses a MLP architecture with sinusoidal time step embeddings with ReLU activation function. The MLP is composed of 3 layers with the hidden dimension of size 1024 and the time step embedding dimension of size 1024. We leverage the ReLU activation function to make the first-order Taylor expansion in Eq. (11) a more accurate approximation. The second derivative of the ReLU activation function is zero, which we expect will minimize the effect of second-order differential terms.

For  $T = 20$ , we use a quadratic scheduler for  $s_t^2$  starting from  $2e - 1$  to  $1e - 1$ . The value function is trained with  $\lambda = 0.95$ ,  $n_{\text{update}} = 1$ , and  $\eta = 1.2$ . The learning rates for the value function and  $\sigma_{\text{init}}$  are set to  $1e - 4$  and  $1e - 3$ , respectively.

The PIS, DIS and DDS is trained using the default setting used in (Berner et al., 2022). We use the code provided at [https://github.com/juliusberner/sde\\_sampler](https://github.com/juliusberner/sde_sampler). The Fourier MLP architecture (Zhang & Chen, 2022) is used, which is fundamentally a MLP architecture with sinusoidal time step embeddings with GeLU activation function. The network is composed of 4 layers with the hidden dimension of size 64 and the time step embedding dimension of size 64. Our VGS algorithm uses KL-divergence based loss. Although both KL-divergence loss and log-variance loss (Richter & Berner, 2024) can be used to train PIS, DIS, and DDS, we chose to use KL-divergence loss to ensure compatibility with the results.

To compute the metrics, we use  $10e5$  randomly sampled data from the target GMM distribution and another  $10e5$  randomly sampled data from a learned sampler.

**Funnel:** Similar to the training of GMM, VGS uses a MLP architecture with sinusoidal time step embeddings with ReLU activation function. The MLP is composed of 4 layers with the hidden dimension of size 1024 and the time step embedding dimension of size 1024.

For  $T = 30$ , we use a quadratic scheduler for  $s_t^2$ , starting from  $5e - 1$  to  $5e - 4$ . The value function is trained with  $\lambda = 0$ ,  $n_{\text{update}} = 3$ , and  $\eta = 1.1$ . The learning rates for the value function and  $\sigma_{\text{init}}$  are set to  $1e - 5$  and  $1e - 3$ , respectively.

The energy of the Funnel distribution diverges as the sampled value of the first dimension,  $x_1$  increases. Extremely high energy values destabilize the training of the value function. To stabilize training, we clip the maximum energy value at 100.

The PIS, DIS and DDS is trained using the default setting used in (Berner et al., 2022) with modification to its training time steps from 60,000 to 10,000 steps as the performance degrades with more steps. The network is composed of 4 layers with the hidden dimension of size 64 and the time step embeddings dimension of size 64.

To compute the metrics, we use  $10e3$  randomly sampled data from the target GMM distribution and another  $10e3$  randomly sampled data from a learned sampler.

**Effect of the Number of Time Steps:** We use the same MLP architecture for VGS with GMM experiment. Noise level of VGS is leveraged by  $s_t^2$  which we use a quadratic scheduler starting from  $5e - 2$  to  $5e - 4$  invariant of time steps  $T$  for low noise level. At each increase of noise level,  $s_t^2$  is increased by doubling the starting point and end point of the  $s_t^2$  scheduler. The value function is trained with  $\lambda = 1 - 0.005T$ ,  $n_{\text{update}} = 3$ , and  $\eta = 1.2$  invariant of noise level. The learning rates for the value function and  $\sigma_{\text{init}}$  are set to  $1e - 4$  and  $1e - 2$ .



Table 4. Training and Sampling time of VGS and baseline models. VGS (128) and VGS (1024) each represents VGS using a value function network with hidden layer dimension of 128 and 1024. VGS (1024) results were used for Table 1. Sampling time was measured for sampling  $10^5$  samples.

Target	Training						Sampling				
	PIS	DIS	DDS	VGS (128)	VGS (1024)		PIS	DIS	DDS	VGS(128)	VGS(1024)
<b>GMM</b>	Parameters	38K	38K	38K	99K	6300K	-	-	-	-	-
	Time	10h	10h	12h	0.40h	<b>0.36h</b>	0.92s	0.94s	1.20s	<b>0.09s</b>	1.90s
<b>Funnel</b>	Parameters	39K	39K	39K	100K	6300K	-	-	-	-	-
	Time	10h	10h	12h	<b>0.75h</b>	1.5h	8.1s	8.3s	10.2s	<b>2.3s</b>	16.4s

### E.3.2. SAMPLING FROM $n$ -BODY SYSTEM EXPERIMENTS

For the  $n$ -body system experiments, we follow the evaluation process used in (He et al., 2024). We use the test set and the evaluation code provided at <https://github.com/jiajunhe98/DiKL> for metric calculation. As in (He et al., 2024), we incorporate early stopping during training, using 2000 validation samples, and save the checkpoint with the lowest TVD-E. For the validation set, we use the validation data from (Akhound-Sadegh et al., 2024). Since the original validation dataset consists of 10k samples, we randomly select 2000 samples.

For testing, the metrics are computed using 2000 samples from our model and the test dataset. We repeat this process 10 times to report the mean and standard deviation. We omit the diffusion step for the final samples and set  $\sigma_{T-1} = 0$  during the evaluation.

**DW-4 (T=30):** For the value function, we use an MLP architecture with sinusoidal time embeddings. The state and time embedding vectors are mapped to a 512-dimensional vector using an MLP, and the concatenated vectors are then passed through a two-layer MLP with a hidden dimension of 512.

For  $s_t^2$ , we use a quadratic scheduler starting from  $1e - 1$  to  $1e - 4$ . We employ the Huber loss for TD updates, as it is known to be less sensitive to outliers. The value function is trained with batch size 512,  $\lambda = 0$ ,  $n_{\text{update}} = 3$ , and  $\eta = 1.2$ . The learning rates for the value function and  $\sigma_{\text{init}}$  are set to  $1e - 5$  and  $1e - 3$ , respectively.

**LJ-13 (T=100):** For the value function, we use an MLP architecture with sinusoidal time embeddings. The state and time embedding vectors are mapped to a 512-dimensional vector using an MLP, and the concatenated vectors are then passed through a three-layer MLP with a hidden dimension of 1024. The final layer input is element-wise multiplied by a time feature vector, which is extracted from a separate network. Motivated by the form of LJ potential, we use the inverse of the pairwise distance as the network input instead of the distance itself. To prevent divergence at  $d = 0$ , a small constant is added.

For  $s_t^2$ , we use an exponential scheduler starting from 0.05 to  $1e - 4$ . We employ the Huber loss for TD updates, as it is known to be less sensitive to outliers. The value function is trained with batch size 512,  $\lambda = 0.9$ ,  $n_{\text{update}} = 3$ , and  $\eta = 1.2$ .

Since the potential of LJ-13 diverges dramatically when two particles are close, we clip the maximum energy value at 100. We also clip the gradient norm during parameter updates at 1.0 for robustness. The learning rates for the value function and  $\sigma_{\text{init}}$  are set to  $1e - 5$  and  $1e - 4$ , respectively. We observed that the LJ-13 potential is highly sensitive to noise and thus reduced the noise scale to  $\eta = 0.9$  during evaluation. When evaluated with  $\eta = 1.0$ , the metrics reported in Table 2 change to TVD-E = 0.294, TVD-D = 0.036,  $\mathcal{W}^2 = 4.283$ .

## E.4. Training and Sampling Time

Table 4 shows the training and sampling time of VGS and SDE-based samplers. Both VGS models show faster training time compared to SDE-based samplers. However VGS (1024) exhibits slower sampling time than SDE-based samplers due to the high computational cost associated with its large number of parameters. In order to make a fair comparison we conducted the same experiment on VGS (128) which has a comparable number of parameters with SDE-based sampler models. VGS (128) showed  $4\times$  faster sampling time compared to SDE-based samplers while maintaining high sampling performance with  $\mathcal{W}_\gamma^2 = 0.021$ , TVD-E = 0.049,  $\Delta\text{std} = 0.107$  for GMM and  $\mathcal{W}_\gamma^2 = 7.457$ , TVD-E = 0.628,  $\Delta\text{std} = 7.658$  for Funnel.

## E.5. Anomaly Detection

## E.5.1. MVTEC-AD

We utilize separate networks for the energy function and the value function, prioritizing the accurate estimation of the energy function. To achieve this, we adopt an autoencoder-based architecture, where the reconstruction error of a sample serves as its energy (Yoon et al., 2021). The diffusion model and the value function are implemented as five-step MLPs with time step embeddings. VGS provides flexibility in selecting  $\pi(\mathbf{x}_0)$ . We initialize the sampler’s distribution by applying noise to the data distribution, enhancing the precision of energy estimation near the data distribution.

Table 5. Total 10 experiments, all models trained for 100 epochs before evaluation. Baselines results are adopted from DxMI (Yoon et al., 2024) paper. The largest value in a task is marked as boldface.

	Detection					Localization				
	Ours	DxMI	UniAD	MPDR	DRAEM	Ours	DxMI	UniAD	MPDR	DRAEM
Bottle	<b>100</b> $\pm 0.00$	<b>100.0</b> $\pm 0.00$	99.7 $\pm 0.04$	<b>100.0</b>	97.5	<b>98.5</b> $\pm 0.02$	<b>98.5</b> $\pm 0.03$	98.1 $\pm 0.04$	<b>98.5</b>	87.6
Cable	<b>97.2</b> $\pm 0.40$	97.1 $\pm 0.37$	95.2 $\pm 0.84$	95.5	57.8	96.7 $\pm 0.06$	96.6 $\pm 0.10$	<b>97.3</b> $\pm 0.10$	95.6	71.3
Capsule	<b>90.8</b> $\pm 0.37$	89.8 $\pm 0.61$	86.9 $\pm 0.73$	86.4	65.3	<b>98.5</b> $\pm 0.01$	<b>98.5</b> $\pm 0.03$	<b>98.5</b> $\pm 0.01$	98.2	50.5
Hazelnut	<b>100</b> $\pm 0.02$	<b>100.0</b> $\pm 0.04$	99.8 $\pm 0.10$	99.9	93.7	98.3 $\pm 0.02$	<b>98.4</b> $\pm 0.04$	98.1 $\pm 0.10$	<b>98.4</b>	96.9
Metal Nut	<b>99.9</b> $\pm 0.06$	<b>99.9</b> $\pm 0.11$	99.2 $\pm 0.09$	<b>99.9</b>	72.8	<b>95.6</b> $\pm 0.04$	95.5 $\pm 0.03$	94.8 $\pm 0.09$	94.5	62.2
Pill	<b>95.7</b> $\pm 0.37$	95.4 $\pm 0.66$	93.7 $\pm 0.65$	94.0	82.2	<b>95.7</b> $\pm 0.03$	95.6 $\pm 0.07$	95.0 $\pm 0.16$	94.9	94.4
Screw	89.7 $\pm 0.79$	88.9 $\pm 0.51$	87.5 $\pm 0.57$	85.9	<b>92.0</b>	<b>98.6</b> $\pm 0.04$	<b>98.6</b> $\pm 0.08$	98.3 $\pm 0.08$	98.1	95.5
Toothbrush	89.5 $\pm 1.47$	92.2 $\pm 1.46$	<b>94.2</b> $\pm 0.20$	89.6	90.6	<b>98.8</b> $\pm 0.02$	<b>98.8</b> $\pm 0.04$	98.4 $\pm 0.03$	98.7	97.7
Transistor	99.1 $\pm 0.37$	99.2 $\pm 0.28$	<b>99.8</b> $\pm 0.09$	98.3	74.8	96.2 $\pm 0.04$	96.0 $\pm 0.13$	<b>97.9</b> $\pm 0.19$	95.4	65.5
Zipper	96.3 $\pm 0.43$	96.3 $\pm 0.50$	95.8 $\pm 0.51$	95.3	<b>98.8</b>	96.8 $\pm 0.12$	96.7 $\pm 0.08$	96.8 $\pm 0.24$	96.2	<b>98.3</b>
Carpet	99.8 $\pm 0.07$	<b>99.9</b> $\pm 0.04$	99.8 $\pm 0.02$	<b>99.9</b>	98.0	98.7 $\pm 0.05$	<b>98.8</b> $\pm 0.02$	98.5 $\pm 0.01$	<b>98.8</b>	98.6
Grid	98.5 $\pm 0.30$	98.6 $\pm 0.28$	98.2 $\pm 0.26$	97.9	<b>99.3</b>	97.1 $\pm 0.05$	97.0 $\pm 0.07$	96.5 $\pm 0.04$	96.9	<b>98.7</b>
Leather	<b>100.0</b> $\pm 0.00$	<b>100.0</b> $\pm 0.00$	<b>100.0</b> $\pm 0.00$	<b>100.0</b>	98.7	98.5 $\pm 0.07$	98.5 $\pm 0.03$	<b>98.8</b> $\pm 0.03$	98.5	97.3
Tile	<b>100.0</b> $\pm 0.00$	<b>100.0</b> $\pm 0.00$	99.3 $\pm 0.14$	<b>100.0</b>	95.2	95.3 $\pm 0.09$	95.2 $\pm 0.14$	91.8 $\pm 0.10$	94.6	<b>98.0</b>
Wood	98.4 $\pm 0.29$	98.3 $\pm 0.33$	98.6 $\pm 0.08$	97.9	<b>99.8</b>	93.9 $\pm 0.08$	93.8 $\pm 0.07$	93.2 $\pm 0.08$	93.8	<b>96.0</b>
Mean	<b>97.0</b> $\pm 0.09$	<b>97.0</b> $\pm 0.11$	96.5 $\pm 0.08$	96.0	88.1	<b>97.1</b> $\pm 0.01$	<b>97.1</b> $\pm 0.02$	96.8 $\pm 0.02$	96.7	87.2